



POLITECNICO DI TORINO

Corso di Laurea in Ingegneria Biomedica

Tesi di Laurea Magistrale

**Sampling and Condensation of
Exhaled Breath Air for the Monitoring
of Viral Load and Lung Diseases**

Relatori

Prof. Guido Sassi

Dott.ssa Maricarmen Leandra Lecuna Tovar

Candidato

Gesualdo Alessia

Anno Accademico 2020/2021

*Alla mia famiglia,
che mi ha sempre sostenuta e incoraggiata.*

Contents

ABSTRACT	3
CHAPTER 1: INTRODUCTION.....	5
1.1. INTRODUCTION TO LUNG DISEASES	5
1.2. LIMITATIONS OF CURRENT DIAGNOSTIC METHODS	8
1.3. NEW DIAGNOSTIC METHODS: EXHALED BREATH AND EXHALED BREATH CONDENSATE ANALYSIS	10
1.4. AIM OF THE WORK.....	12
1.5. OBJECTIVES OF THE WORK	13
CHAPTER 2: METHODS	15
2.1. THERMODYNAMIC EQUILIBRIUM	15
2.2. THERMODYNAMICS MODELS.....	17
2.2.1. <i>Equation of State Models</i>	17
2.2.2. ACTIVITY COEFFICIENT MODELS	18
2.3. LIMITS OF STANDARD THERMODYNAMIC MODELS AND POSSIBLE ALTERNATIVES	18
2.4. CONDENSATION PROCESS SIMULATION IN REAL CONDITIONS	20
2.5. CALCULATION TOOLS	20
CHAPTER 3: STATE OF THE ART OF THE EBC ANALYSIS METHOD.....	22
3.1. SEARCHES TO DEFINE THE STATE OF THE ART	22
3.2. BIBLIOMETRIC ANALYSIS	23
3.3. BIOMARKERS CONNECTED TO LUNG DISEASES	24
3.4. SAMPLING METHODS	26
3.4.1. <i>Respiratory Volumes and Capacities</i>	26
3.4.2. <i>Condensing Devices</i>	28
3.4.3. <i>Sampling Challenges</i>	30
CHAPTER 4: CONDENSATION PROCESS SIMULATION IN THERMODYNAMIC EQUILIBRIUM CONDITION.....	32
4.1. EXHALED AIR COMPOSITION OF A HEALTHY SUBJECT USED FOR THE SIMULATION	32
4.2. THERMODYNAMIC PROPERTY METHODS USED FOR ASPEN SIMULATIONS.....	34
4.3. CONDENSATION PROCESS SIMULATION SETUP.....	36
4.3.1. <i>Aspen Sensitivity Analysis Setup</i>	37
4.4. UNCERTAINTY BUDGET COMBINED UNCERTAINTY ESTIMATION	40
4.4.1. <i>Estimation of Condensate Volume Uncertainty</i>	41
4.4.2. <i>Estimation of Uncertainty of the Ammonia Molarity in the Exhaled Breath Condensate</i>	42
4.5. CONDENSATION PROCESS SIMULATION RESULTS	42
4.5.1. <i>Condensate Volume Evaluation</i>	42

4.5.2. <i>Yield of Every Components of Exhaled Air After Condensation Process</i>	43
4.5.3. <i>Sensitivity Analysis Results</i>	51
4.5.4. <i>Results of Uncertainty Budget</i>	56
CHAPTER 5: CONDENSATION PROCESS SIMULATION IN REAL CONDITION: CFD SIMULATION.....	59
5.1. SIMULATION OF CONDENSATION PROCESS IN LITERATURE	60
5.2. CFD SIMULATION WITH SMALL DIMENSION GEOMETRY	61
5.2.1. <i>Geometric Model and Mesh</i>	61
5.2.2. <i>CFD Simulation Setup in ANSYS Fluent</i>	62
5.3. CFD SIMULATION WITH REAL DIMENSION GEOMETRY	64
5.3.1. <i>Geometric Model and Meshing</i>	64
5.3.2. <i>Mesh Verification and Validation</i>	65
5.3.3. <i>CFD Simulation Setup in ANSYS Fluent</i>	66
5.4. RESULTS OF CFD SIMULATION IN ANSYS FLUENT	67
5.4.1. <i>Results of CFD Simulation with Small Dimension Geometry</i>	67
5.4.2. <i>Results of Mesh Validation</i>	68
5.4.3. <i>Results of CFD Simulation with Real Dimension Geometry</i>	70
CHAPTER 6: CONCLUSIONS AND FUTURE DEVELOPMENTS.....	73
APPENDIX A: VOCs AND NON-VOLATILE BIOMARKERS FOR LUNG DISEASES.....	75
APPENDIX B: CHARACTERISTICS OF EXHALED BREATH COLLECTING AND CONDENSING DEVICES ON THE MARKET AND SELF-MADE.....	78
BIBLIOGRAPHY.....	83
SITOGRAPHY	90

Abstract

The pandemic of 2020 caused by the coronavirus Sars-CoV-2 involves problems with the respiratory system and has already caused 2 million deaths worldwide. Respiratory diseases are the third leading cause of death in the world. Lung cancer is the cancer with the highest incidence of death and it is widespread among adults and children. For a successful treatment of lung diseases, it is essential to early diagnose them and follow the patient constantly during the disease progress, however, current diagnostic tools are invasive and lack accuracy and reproducibility.

A promising method to diagnose and monitor pulmonary diseases is the Exhaled Breath Condensate (EBC) analysis, which allows to trace exhaled Volatile Organic Compounds (VOCs) considered as biomarkers of those pathologies. The EBC analysis method has lots of positive aspects: it is totally non-invasive, it is easy to perform with patients of all ages and with every respiratory disease, independently of their severity, and it is useful for serial longitudinal and epidemiological studies. Unfortunately, it is not yet widely used in clinical practice due to a lack of agreement on the biomarkers profiles for each disease, related to large uncertainties and a lack of standardization and validation of breath samples collection. Low concentrations of the different biomarkers make this kind of analysis a metrological challenge. Due to the nature of the EBC method, the aerosols and droplets in expired breath are collected and with this liquid also the total viral material expired. This characteristic is important not only for the diagnosis of viral diseases but also for the understanding of the spreading risks associated to expired breath of subjects carrying Sars-Cov-2 and others virus.

Thus, the purpose of this thesis is to model a EBC sampler to diagnose lung diseases, using Aspen HYSYS and ANSYS Fluent. Validation of the model was performed against literature data. After the simulations, we focus our attention on how much condensate volume is obtained from a volume of exhaled air in Fluent and Aspen and on the composition of the exhaled breath condensate in Aspen. In particular, the ammonia concentration in exhaled air and in the EBC was analysed through sensitivity analyses. To compare the literature reference value of ammonia molarity in the condensate and the condensate volume with the results obtained from the simulations, an estimation of the uncertainty following the GUM (Guide for the Expression of the Uncertainty in Measurement) was performed. The Computational Fluid Dynamics (CFD) simulation in Fluent was used to evaluate the air condensation in the chosen geometry and the heat exchange areas.

From these analyses, it emerges that the condensate volume is in line with the values found in the literature. The concentration of ammonia in the EBC was highly dependent on the model used, although it could not be validated since the available data had an already large variability.

Chapter 1: Introduction

1.1. Introduction to Lung Diseases

Lung diseases are widespread in both adults and children and each pathology is associated with clinical challenges, which make them still interesting from a research point of view [1]. According to data from the World Health Organization, chronic obstructive pulmonary disease (COPD) caused the death of 3 million people in 2016, ranking as the third leading cause of death in the world, while lower respiratory tract infections caused nearly 3 million deaths in 2016, as shown in Figure 1 [I]. Lung cancer, along with cancer of the trachea and bronchial tubes, caused 1.76 million deaths in 2018 and was the cancer with the highest incidence of death (Figure 2) [II].

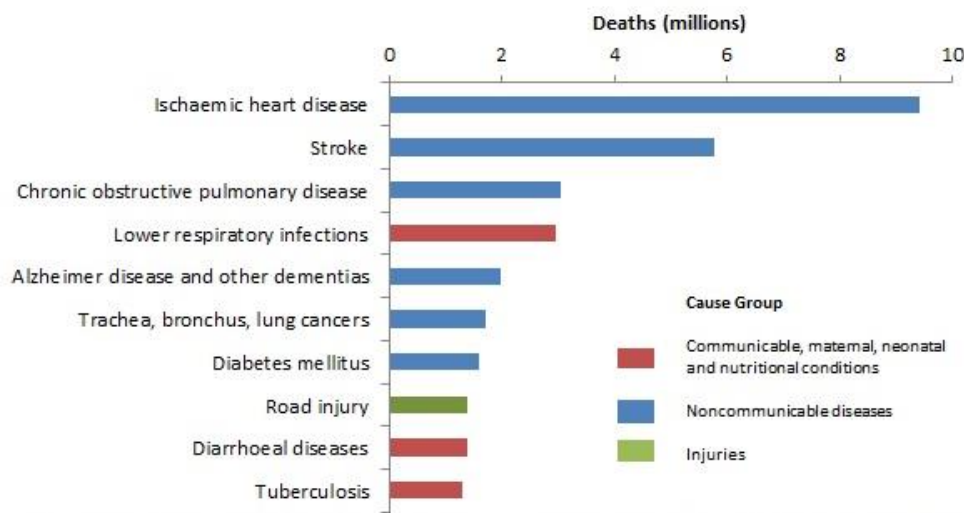


Figure 1. Top 10 global causes of death in 2016 [I].

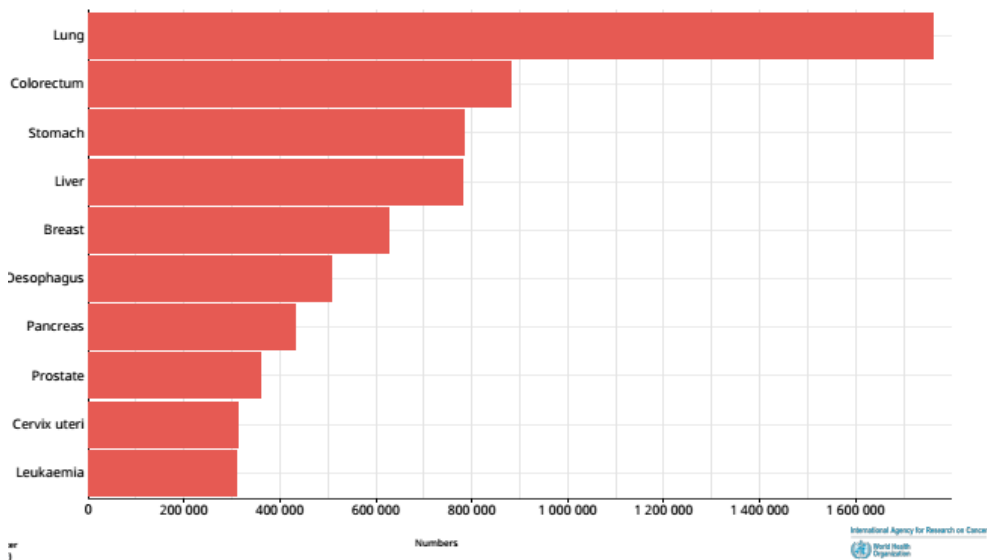


Figure 2. Number of deaths worldwide, both sexes, all ages in 2018 [III].

Lung diseases can be classified into diseases involving inflammation and oxidative stress of the airways and infectious diseases, caused by viral or bacterial pathogens. Among the first, which may be chronic or not, we can find:

- Bronchial asthma: it is a chronic and multifactorial syndrome that affects adults and children, causes reversible obstruction of the airways through spasms, inflammation, and excessive secretion induced by mast cells and also involves bronchial hyperreactivity to minimal stimuli. The inflammatory state associated with this pathology is characterized by the infiltration of eosinophils and T helper 2 (Th2) lymphocytes into the submucosa [2] [3];
- COPD (chronic obstructive pulmonary disease): is a very common disease, which can be prevented and treated, characterized by inflammation of the airways and progressive and persistent limitation of air flow; the latter is caused by the rupture of lung tissue (emphysema) and obstructive bronchiolitis, an inflammation of the bronchioles [4];
- Cystic fibrosis: it is an autosomal recessive genetic disease that involves the cells that produce mucus and sweat; in particular, the mutation of a gene causes the change of a protein that regulates the activity of sodium and chlorine channels on the cell surface. The result of this mutation is the production of thick, sticky, water-poor mucus that clogs the airways and traps bacteria, the most common being *Pseudomonas Aeruginosa*, which cause infections, inflammation, respiratory failure and other complications. [5] [IV] Infection and inflammation are chronic and involve the presence of many neutrophils and cytokines in the secretions of the airways [6];
- Lung cancer: the respiratory system can be the site of primary tumors or metastatic localizations of tumors that have arisen in other sites; the most spread tumors is lung cancer, a malignant primary neoplasm, that has several histological varieties [7];
- Bronchiectasis: are suck-like dilatations of bronchi and bronchioles wall that obstruct the air passage for the formation of vortices or for the mucus stagnation. The formation of bronchiectasis is often due to long-lasting infections; [7]
- Interstitial lung disease (ILD): refers to more than 200 chronic lung disorders; with ILD, the tissue between the alveoli (the interstitium) is affected by inflammation or scarring (fibrosis), this causes breathing difficulties because lung tissue becomes stiffer [V].

Among the infectious respiratory diseases, we find:

- Chronic bronchitis: are chronic or acute inflammatory processes of the mucous lining of the large bronchi caused by pathogens; during bronchitis, the air passage through the airways is reduced due to the presence of exudate in it or to the increase in mucus secretion; [7]
- Pulmonary sarcoidosis: is a chronic inflammatory granulomatous disorder with an unknown etiology that cause respiratory failure. This pathology, in addition to the lung, can involve the lymph nodes, spleen, liver, skin, salivary and lacrimal glands, bones and joints; [7]
- Acute respiratory distress syndrome (ARDS): is a lung condition that causes low blood oxygen because fluid builds up in alveoli and surfactant breaks down; these changes limit the exchange of oxygen and carbon dioxide in the alveoli. The ARDS follows the lung infections that cause the alveoli damage [VI];
- Viral infections: these infections include influenza, cold, but also pneumonia and bronchopneumonia. The viruses responsible for colds are adenoviruses, coronaviruses, human meta-pneumoviruses (hMPVs) and rhinoviruses [VII], while influenza is caused by viruses belonging to the orthomyxoviridae family, divided into A, B and C type [VIII].

Among the viral infection it is important to consider the novel coronavirus pneumonia, COVID-19, caused by the novel coronavirus, initially named 2019-nCoV and later renamed Sars-CoV-2 [8], IX]. The outbreak of this novel pneumonia started at the end of 2019 in Wuhan, China, and has spread rapidly to other countries [8]; because of this, with more than 118.000 cases in 114 countries, and 4.291 deaths, the 11 March 2020 the World Health Organization (WHO) has declared that COVID-19 can be characterized as a pandemic [X]. The most common symptoms of COVID-19 are fever, cough and myalgia or fatigue; less common symptoms are sputum production, headache, haemoptysis, and diarrhoea [9]. Now, Sars-CoV-2 is worldwide spread and the most updated data on its diffusion are shown in the table below (Table 1).

GEOGRAPHIC AREA	CONFIRMED CASES	DEATHS
Global	103.631.793	2.251.613
Americas	46.197.580	1.068.110
South-East Asia	12.956.439	199.291
Europe	34.658.178	759.122
Eastern Mediterranean	5.759.214	135.811
Africa	2.603.698	63.940
Western Pacific	1.455.939	25.326

Table 1. Confirmed cases and deaths of Sars-CoV-2 infection, updated to 04/02/2021 [XI].

1.2. Limitations of Current Diagnostic Methods

It is essential to early diagnose these diseases and follow the patient constantly during the disease progress, to reduce this pathology mortality and the health care costs. Current diagnostic tools are often not satisfying and invasive.

For example, lung cancer is often diagnosed at an advanced stage, when the first symptoms have already appeared and successful treatments are difficult [1]. In the case of children with asthma, a reliable diagnosis is difficult because there are no tools available to discriminate between true asthmatics and children with transient, viral infections symptoms [1]. In asthmatic patients the “gold standard” for measuring inflammation in the airway wall is fiberoptic bronchial biopsies, but this is an invasive procedure, not suitable for routine clinical practice; it is also unsuitable for use in children and patients with severe diseases [10].

Some of the techniques used to diagnose these lung diseases and monitor infection and inflammation over time are:

- Bronchoscopy: is one of the oldest invasive medical techniques used in respiratory and thoracic field; can be done with a rigid bronchoscope, a stainless-steel tapered tube, or with a flexible bronchoscope and both of them have a illumination and visualization system of the airway [11]. The first type of bronchoscope is now used only in a few applications, while the latter is the most used, also because it requires less anaesthesia, and it does not have the typical limitations of a rigid instruments [12]. This tool is both a diagnostic and a therapeutic tool [11];
- Transbronchial lung biopsy: is an invasive method for obtaining histologic tissue of the lung to diagnose diseases and infections; it is performed during a standard bronchoscopy, with or without fluoroscopy, with a flexible fiberoptic bronchoscope, under moderate sedation [12];
- Bronchoalveolar lavage (BAL): is an invasive method used to obtain cytological material from the lower respiratory tract and alveoli; it is performed by injecting sterile saline into the duct of a flexible bronchoscope and subsequent suction is applied to recapture the instilled fluid. BAL fluid analysis is performed to diagnose infections, inflammations, and malignant diseases and to evaluate the cellular response to lung diseases; [12]
- Endobronchial sputum analysis: is a non-invasive method of sampling biomarkers to evaluate pulmonary diseases severity

and progression, including exacerbations; not all patients can produce spontaneous sputum samples and that is a limit [13];

- Induced sputum analysis: this technique is a little invasive as it consists of inhalation of hypertonic saline to induce sputum; the sputum sample collected is then analysed to quantify inflammatory cell and mediators in a relatively reproducible way. This practice may induce coughing, bronchoconstriction, is difficult to use in small children and itself induces an inflammation response. [10]

As to COVID-19, the gold standard for confirming Sars-CoV-2 infection is real-time reverse transcriptase–polymerase chain reaction (rRT-PCR) of nasopharyngeal swabs to identify viral RNA [14]. There are also other methods to detect the novel coronavirus infection like sputum, bronchoalveolar lavage fluid (BALF) [8] and saliva [15]. Yang et al. [8] have evaluated the most suitable method to diagnose COVID-19 concluding that, except for BALF, that is the most accurate but invasive method, sputum may serve as the most sensitive samples, followed by nasal swabs; however, only a small portion of novel coronavirus pneumonia cases showed sputum production.

Nasopharyngeal swab, although less invasive than BALF, is a semi-invasive test too because it is performed inserting the swab through the nostril parallel to the palate until resistance is encountered, indicating contact with the nasopharynx (Figure 3); then is necessary to rotate, rub and leave the swab in place for several seconds and, at the end, the swab is slowly removed while rotating it [XII].

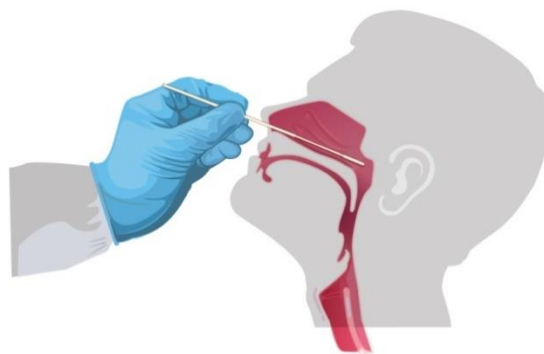


Figure 3. How to perform a nasopharyngeal swab [XII].

Moreover, this test requires lengthy procedures and many bio-agents, and it often leads to false negatives [16]. The swab is highly specific for SARS-CoV-2, as it is not positive when exposed to the nucleic acid of other viruses; while the in vitro sensitivity of RT-PCR tests is high, but in clinical settings the sensitivity is moderate, and this means that a negative test does not rule out the disease [17].

1.3. New Diagnostic Methods: Exhaled Breath and Exhaled Breath Condensate Analysis

A promising diagnostic method is the exhaled breath (EB) analysis to track down volatile organic compounds (VOCs) profile and to identify specific biomarkers of pulmonary diseases. This method is non-invasive, it can be used many times, in patients with severe disease, and to monitor disease in children and infants [10]. This technique could be useful for monitoring inflammation in the lungs, diagnose pulmonary diseases, monitoring response to treatment [10] and diagnose viral airway infection [16].

EB methods consist in the collection, detection and analysis of exhaled VOCs, that are a diverse group of carbon-based chemical compounds, volatile at room temperature, formed in the body during (patho)physiological processes; these non-polar, polar, or highly polar components, with smaller molecular size, are in the liquid state when they are pure, but they easily pass into the gaseous state due to their high vapor pressure [1] [18].

After the collection of the exhaled breath samples, they can be analysed with gas chromatography (GC), the gold standard, followed by mass spectrometry (GC-MS) or flame ionization detection (GC-FID) or with an e Nose, an array of nano-sensors. During the analysis of EB samples researchers can focus on either single compounds or on VOCs profiles [1].

Van de Kant et al. [1] in their review maintain that a combination of VOCs, ranged from 7 to 33 identified by GC-MS, could differentiate lung cancer patients from controls; with a sensitivity of 50-100% and a specificity of 80-100%. Chen et al. [16] have used a commercial breath VOC analyser to search specific biomarkers for COVID-19, that can rapidly screen COVID-19 patients from healthy subjects, in a non-invasive way, even before the development of symptoms; for the analysis of the samples, they have used a gas chromatograph (GC) and an ion mobility spectrometer (IMS).

VOCs can be evaluated not only directly from the analysis of the exhaled air, but also through the analysis of the exhaled breath condensate (EBC); this is a non-invasive method of sampling the airways because the condensate contains water and aerosolised particles from the airway lining fluid (ALF), generated from the entire respiratory tract (from mouth to alveolus) [19]. EBC does not collect respiratory cells but contains biomarkers whose concentration is influenced by these cells: an alteration in concentration represents a change in the cellular activity. During the condensation process some components pass to the liquid state by condensation and other

VOCs, for example ammonia, dissolve in water, which is the major condensable component of the exhaled air.

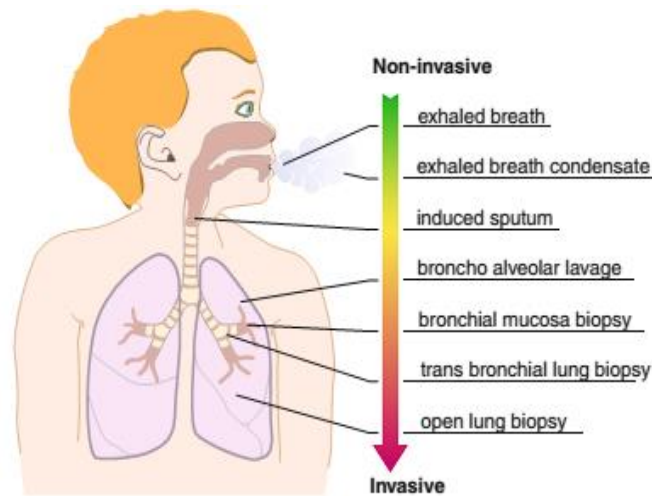


Figure 4. Methods to access airway inflammation, infection, and pulmonary diseases [1].

The EBC sample is collected with various type of collection devices, commercial or custom-made, but all devices function by cooling exhaled breath; it condenses into either liquid or ice depending on the cooling temperature. [20]

Corradi et al. [21] in their study have analysed aldehydes levels in exhaled breath condensate of patients with stable COPD compared with those of smoking and non-smoking control subject using liquid chromatography-tandem mass spectrometry. They have identified some classes of aldehydes that are increased in the EBC of patients with COPD in comparison with non-smoking control subjects [21]. Mendes et al. [22] in a research study have evaluated eleven miRNAs in EBC as potential biomarkers to diagnose asthma in school aged children; the EBC samples were used as an alternative to induced sputum and were analysed by reverse transcription-quantitative real-time PCR. They concluded that EBC is feasible, simple, safe, and non-invasive and EBC miRNA profile is useful to identify asthma [22]. Also, Pattnaik et al. [23] in their review say that there is an involvement of miRNAs in pulmonary sarcoidosis. EBC analysis could be promising also in the detection of COVID-19 infection because the virus spreads via respiratory droplets; condensate is also similar with bronchial lavage fluid (BLF) for biochemical contents and origin of production, whose analysis with RT-PCR is the most accurate method to detect Sars-CoV-2. Despite BLF, collection of EBC is simple, well tolerated, non-invasive and has no adverse effects, therefore it could be employed as many times as needed in follow-up investigations of patients [24].

The table below shows advantages and limitations of EB analysis despite traditional methods [25] [26] [27]:

ADVANTAGES	LIMITATIONS
Totally non-invasive, it does not require any intervention through the respiratory tract	Lack of standard method to collect breath samples
Is available for use in all ages and in patient with every respiratory disease independently of their severity even in mechanically ventilated patients	Not yet used in clinical practice, standardization and validation is still needed
Simple and easy to perform, it does not require special personnel or distinct knowledge	There may be a concentration artefact due to evaporation of water
The equipment used for its collection is very simple and relatively cheap	Low concentration range of different biomarkers (metrological challenge)
Useful for serial longitudinal and epidemiological studies because it can be repeated several times	The collected fluid is not anatomic-site specific

Table 2. Advantages and limitation of EC analysis.

1.4. Aim of the Work

The purpose of this thesis is to model an exhaled breath sampling and condensation system to diagnose lung diseases, aimed to the design of a first prototype. Starting from a profile of volatile substances present in the exhaled breath, simulations will be run to optimize the condensation parameters. The quantification of the composition of the liquid sample obtained with these simulations will be used for accessing the presence of profiles of volatile organic substances and non-volatile compounds identified as biomarkers of lung cancer and Sars-CoV-2 infection. The liquid sample obtained can be analysed also by PCR for discovering the presence of viral infection and for the quantification of the viral load in exhaled breath.

The measurement of biomarkers of lung diseases is linked to the sampling of exhaled air and condensate, to the biomarker measurement itself, that is connected to the measuring instrument used to evaluate the air components quantity in the condensate and to the reference with a standard to evaluate the reproducibility of measurements; in particular, this thesis work focuses on the sampling of exhaled air and condensate.

To start this work, we need to know which diseases other research groups have tried to recognize with this technique, to choose which

pathologies to focus on and which profiles of VOC and then biomarkers consider. It is also necessary to know which collection and condensation systems are now on the market or which custom-made devices have been used in the past by other researchers to evaluate if there are possibilities for improvement and to understand the condensation conditions they considered. Finally, it is essential to investigate the current challenges of EBC sampling and analysis.

The thesis work continues trying to aggregate the data present in the literature with each other, as it was realized that complete studies, that start from the exhaled breath composition of healthy or pathological subjects and arrive at the evaluation of the condensed breath composition, both in a simulated and experimental way, are not present. In particular, we look for the best thermodynamic model for the air condensation process, to obtain the best fit with the literature data and to perform a validation.

With this aim, the volume of condensate, the maximum theoretical yield of air components in the condensate, and the thermal exchange area were evaluated with a series of simulations using Aspen HYSYS and ANSYS Fluent software, even if there are limits on the choice of the property method due to the possible formation of solid phase during the air condensation process at low temperatures, not taken into account by the software and to the lack of data in literature on the condensation process simulation parameters used.

1.5. Objectives of the Work

The objectives of this work are listed below.

Research the EBC analysis method in the scientific literature to define the state of the art. The research is done focusing on which are the most studied lung diseases with the EBC analysis method (bibliometric analysis), the biomarkers connected to lung diseases, volatile and non-volatile compounds, the pulmonary volumes, normal and pathological, the commercially available sampling devices and the researcher-built experimental samplers and the sampling challenges.

Study the condensation upon reaching equilibrium of the system for **evaluate** the maximum theoretical yield of each air component in the condensate and the volume of condensate. **Choose** the best thermodynamic model to describe the condensation process and evaluate the problems to perform a good simulation of a condensation process, which considers the condensation of VOCs, the condensation of other air components, and the water

solubilization of some of them. To achieve this goal a simulation of a condensation process was carry out using the software Aspen Plus V10.

Analyse the exhaled breath condensation process from a fluid dynamics point of view in similar to reality conditions after choosing a thermodynamic model and **evaluate** under what conditions of geometry and heat exchange areas it is possible to reach a situation as close as possible to equilibrium. To achieve this goal a CFD simulation in ANSYS Fluent was performed using an air-water system. A quality check of the mesh has also been provided, comparing the results of the CFD simulation as the mesh changes, for the chosen geometry.

Chapter 2: Methods

In this chapter we will be introduced to the theoretical methods on which this thesis work is based. The concept of thermodynamic equilibrium is the starting point, which sets a theoretical limit to the obtainable results, which cannot be exceeded. The concept of the thermodynamic model was then illustrated and the most widespread thermodynamic models, fundamental for describing the properties of mixtures and components, were presented. Finally, the theoretical basis for describing the condensation process in real conditions will be presented. The calculation tools, used to perform all the analyses carried out to achieve the set objectives, will also be presented.

2.1. Thermodynamic Equilibrium

When thermodynamic equilibrium occurs, “there is no tendency for the state of a system to change spontaneously and its properties do not change with time” [28], that is, there is the equality of the potential between the two parts of the system:

$$Pot, \alpha = Pot, \beta$$

During thermal equilibrium there is temperature equality and in case of chemical equilibrium there are no diffusion phenomena or chemical reactions and the composition of the phases of the system remains constant over time.

The equilibrium is a thermodynamic limit beyond which one cannot go; equilibrium is established between the phases and depends on the pressure, the temperature, and the molar concentration of the phases of the system; with the same parameters, after reaching equilibrium, the composition of the phases does not vary.

To describe the thermodynamic equilibrium, it is necessary to define the properties of the phases at equilibrium and the equilibrium equations that can be used. There are many of them and a discriminating factor is the number of phases present and the presence of a solid phase, which radically change the way properties are calculated for the single substances.

One equilibrium equation is enough to describe the equilibrium between a liquid and a vapour; instead, if there are two liquid phases (organic and aqueous phases) and a vapour phase it is necessary to consider the interactions between the three phases with three equilibrium equations. Within each single phase there may be other reactions, with their equilibrium constant; generally, the reactions in the organic phase are not considered, while those in the aqueous

phase, such as acid-base reactions due to the presence of polar components in water, can influence the equilibrium of the system and are considered with their own equilibrium equation.

For the air condensation in a liquid mixture, the equilibrium is governed by Raoult's law and by Henry's law, which are based on the fact that, in an equilibrium state of the system, the chemical potential of a substance present in the vapor state must equal the chemical potential of the corresponding liquid [29].

The first states that the ratio between the partial vapor pressure of each component in the gaseous phase (p_i) and the corresponding vapor pressure in the pure liquid ($p_{V,i}$) is equal to the molar fraction of the component in the liquid mixture (x_i):

$$p_i = x_i * p_{V,i}(T)$$

The partial vapor pressure of each component in the gaseous state is calculated as the product of the total pressure (p_{tot}) and the fraction of that component in the gaseous state (y_i):

$$p_i = y_i * p_{tot}$$

Both the solute and the solvent of ideal solutions follow the condensation equation of Raoult. An ideal solution is composed of pure substances, for which the interactions between two components are similar to the interaction of a component with itself.

If the solution is not ideal it is necessary to calculate and insert in the equation an ideality coefficient $i(T, x_i)$, which depends on the temperature and the solution composition, since it takes into account that all the components in solution react with the component i .

Raoult's law for real solution takes the following formulation:

$$y_i * p_{tot} = i(T, x_i) * x_i * p_{V,i}(T)$$

Henry's law is an empirical solubilization equation that states that the partial pressure of the solute in the gas phase (p_i) is proportional to its mole fraction in solution (x_i) and to a constant of empirical proportionality of the size of a pressure:

$$y_i * p_{tot} = x_i * H(T)$$

Mixtures that obey Henry's law and Raoult's law are called ideal dilute solutions, for which solute-solute interactions are negligible. [29]

These equations are valid for exhaled breath condensate, which is a dilute solution consisting of 99.9% of water and well describe this process because air is formed by volatile components that do not condense, but dissolve in a solvent and by components that condense and form mixtures in solution.

2.2. Thermodynamics Models

To describe the equilibrium of a multiphase system, thermodynamic models are used to calculate the properties of pure components and mixtures and their definitions are a central point in the modelling of a thermodynamic system; they are based on Raoult's law and Henry's law.

They are divided in equation-of-state methods, with which all properties for both phases can be derived from the equation of state, and activity coefficient methods, with which the vapor phase properties are derived from an equation of state and the liquid phase properties are calculated from the pure component properties [30].

2.2.1. Equation of State Models

An equation of state is a thermodynamic equation that indicates the relationship between two or more state variables, such as temperature, pressure, volume, or internal energy.

The most common equations of state property methods are based on ideal gas law, Peng-Robinson and Soave-Redlich-Kwong standard equation of state.

The ideal gas law is the simplest equation of state and relates the pressure (P), the volume (V), the temperature (T) and the amount of substance (n) through the universal gas constant (R):

$$P * V = n * R * T$$

$R = 0.08205 \text{ [(atm*L) / (mol*K)]}$. [31]

“The ideal gas law assumes that molecules have no size and that there are no intermolecular interactions, and this can be called absolute ideality” [30], therefore it approximates the behaviour of real gases at low pressures and high temperatures [31].

The Peng-Robinson equation of state models a non-ideal system by relating P, V and T with the following equation:

$$P = \frac{RT}{(c + V_m) - b} - \frac{a(T)}{(V_m + c)(V_m + c + b) + b(V_m + c - b)}$$

Where a, b, and c are component specific parameters [32].

The Soave-Redlich-Kwong equation of state models a non-ideal system due to compressibility effects by relating P, V and T with the following equation:

$$P = \frac{RT}{(V_m - b)} - \frac{a(T)}{V_m(V_m + b)}$$

Where a and b are component specific parameters. [30]

2.2.2. Activity Coefficient Models

As regards the activity coefficient models, the NRTL (Non-Random Two-Liquid), UNIQUAC (Universal Quasichemical), WILSON models and their variances are the most used and they are all suitable for simulations with non-ideal mixtures formed by non-electrolyte and polar components, at a pressure below 10 bar [33].

These models use an equation of state to predict the properties of the gas phase and involve the use of Henry's law to model incondensable components [30], but WILSON models only the liquid-vapor equilibrium while the other two model both the liquid-vapor equilibrium and liquid-liquid equilibrium [33][53]. These models differ in the value they assign to binary interactions parameters and in the parameters use to calculate the activity coefficient, derived from experimental data stored in data banks [30]

Another activity coefficient model for simulate the condensation equilibrium is the Electrolyte NRTL models, which considers ionic reactions and interactions (molecule-ion and ion-ion) due to the dissociation of electrolytes into ions in solution; this method uses an equation of state for calculate all vapor phase properties [30].

2.3. Limits of Standard Thermodynamic Models and Possible Alternatives

All the equilibrium models operate an approximation of the real situation and for this reason they are sometimes not very precise in describing the phenomenon of interest. In the case of the simulation of the condensation process, the models above, the standard thermodynamic models, did not allow to model the formation of solid in the condenser, but the solid phase formation is plausible due to the high water content in the EBC and the condensation temperature below 0°C.

Among the models that allow to model even the solid phase, there are those used to describe the process of freeze-drying, a method to remove water from an organic substance to obtain the organic components with the minimum possible deterioration.

They can be divided into, multidimensional and monodimensional models and they have the aim to estimate the product temperature on the basis of the saturating vapour pressure of the ice: the former are quite complex, and their numerical solution can be highly time-consuming, the latter make simplifying assumptions but can be adequate to represent the system [34].

The most common mathematical models, used for describing the freeze-drying process are Manometric Temperature Measurement (MTM) algorithm, Dynamic Pressure Rise (DPR) algorithm, Pressure Rise Analysis (PRA) algorithm and Dynamic Parameters Estimation (DPE) algorithm. These methods differ, among other things, for the relation between the temperature of the sublimation interface and the vapour pressure of water over ice, that is required to implement these methods [35].

These relations are all based on the Goff-Gratch equation, that covers a range from -100°C to =°C, used as it is in the DPE algorithm and modified for the range of interest for the other algorithms [XIII] [35]. The formulation of these equations, obtained by interpolating the experimental data, are reported below:

DPE algorithm (Goff-Gratch equation):

$$p_{w,i} = 100 * \exp \left[-9,09718 \left(\frac{273,16}{T_i} - 1 \right) - 3,56654 \log_{10} \left(\frac{273,16}{T_i} \right) + 0,876793 \left(1 - \frac{273,16}{T_i} \right) + \log_{10} 6,1071 \right]$$

$$\text{MTM algorithm: } p_{w,i,\text{MTM}} = \frac{101325}{760} * \exp \left(-\frac{6144,96}{T_i} + 24,01849 \right)$$

$$\text{PRA algorithm: } p_{w,i,\text{PRA}} = \exp \left(-\frac{6320,1517}{T_i} + 29,5578 \right)$$

$$\text{DPE algorithm: } p_{w,i,\text{DPE}} = \exp \left(-\frac{6140,4}{T_i} + 28,916 \right)$$

Where T_i = temperature of the sublimation interface [K]

$p_{w,i}$ = vapour pressure of water over ice [Pa]

[35]

2.4. Condensation Process Simulation in Real Conditions

To evaluate under what conditions of geometry and heat exchange area it is possible to reach a situation as close as possible to equilibrium, the condensation process was also evaluated with a Computation Fluid Dynamics (CFD) simulation using an air-water system.

CFD simulations are a calculation tool that allows to analyse and solve problems that involve fluid flows using numerical analysis using a finite volume system to perform a zone-by-zone calculation. With this method, the governing partial differential equations, the Navier-Stokes equations, the mass, momentum and energy conservation equations are solved over discrete control volumes, represented by geometry that has been discretized with a mesh, in an iterative way.

Instead of the simulations in Aspen, the CFD simulations allows us to simulate the performance of condensation heat transfer in presence of noncondensable gases. The heat transfer, which regulates the real condensation process, takes the following generic formulation:

$$q = U * A * \Delta T$$

Where q = transmitted thermal power, the heat flow

U = coefficient of global heat exchange

A = area of the heat exchange surface

ΔT = temperature gradient.

2.5. Calculation Tools

In this thesis work, the equilibrium state between the system's phases is evaluated using Aspen Plus V10 as calculation tool. Setting a continuous input flow, with a certain composition, which simulates the human breathing, this software gives a thermodynamic equilibrium between the output phases, which allows to calculate the theoretical maximum yield of the exhaled air condensation process.

Aspen allows to perform a thermodynamic equilibrium between the liquid phase, the condensate and the gas phase, the air or between a gas phase and two liquid phases as the temperature and the pressure change and as the property method, that is the thermodynamic model vary.

It was chosen this software because it had the property methods already tested in it, which allowed to avoid calculation errors that we could have made using other tools and it uses international data bases, tested, and checked, to calculate the activity coefficients and the interactions between the phases and their components. Aspen,

however, has the limit of not being able to use property methods that model the solid phase.

The CFD simulation was performed using fluent ANSYS software, widely used both in academic and industrial fields, which allows to model flows, turbulence, heat transfer and reactions chemists by evaluating the conservation equation of mass, momentum, and energy for each single element of the mesh.

Chapter 3: State of the Art of the EBC Analysis Method

In this chapter the state of the art of EBC analysis will be presented: the most studied lung diseases with the analysis of EBC and the main biomarkers related to these diseases were researched; an analysis of lung volumes and capacities and of the devices on the market to sample exhaled air was performed; finally, the current challenges and limits of sampling and condensation of the exhaled air were analysed.

3.1. Searches to Define the State of the Art

The first step of this work was a bibliometric analysis to identify the most studied lung diseases with this technique. A systematic search of the PubMed database and Proquest database was performed to extract information of the last ten years, excluding abstract-only studies, using the following search terms in abstract and title only:

- ["Exhaled breath condensate"];
- ["Exhaled breath condensate" AND "chronic obstructive pulmonary disease"];
- ["Exhaled breath condensate" AND "cystic fibrosis"];
- ["Exhaled breath condensate" AND "asthma"];
- ["Exhaled breath condensate" AND "lung cancer"];
- ["Exhaled breath condensate" AND "bronchiectasis"];
- ["Exhaled breath condensate" AND "sarcoidosis"];
- ["Exhaled breath condensate" AND "Acute Respiratory Distress Syndrome"];

Then a bibliographic research was performed on PubMed database to understand the use of EBC analysis connected to viral infections, using "exhaled breath condensate", "exhaled breath analysis", "viral load", "viral infections" and "COVID-19" as keywords in all fields.

To define the state of the art of EBC analysis method also a bibliographic research on PubMed and Proquest databases was carried out to find VOCs and non-volatile compounds to consider as lung diseases biomarkers. Initially, only reviews were taken into consideration and then the research was extended to research articles; "VOCs", "biomarkers" and "EBC" were used as keywords. In these reviews there was also information about EBC sampling challenges.

In the end, the commercial-available sampling devices and the researcher-built experimental samplers were researched in the same

databases previously used, in order to make a comparison between their main characteristics.

3.2. Bibliometric Analysis

The results of the bibliometric analysis, summarized in the table below (Table 3), show that the most studied diseases with the exhaled breath analysis are: asthma, COPD, lung cancer and cystic fibrosis. These are all diseases linked to inflammation and oxidative stress, whose biomarkers are present in the EBC.

According to van de Kant et al. [1] there is heterogeneity between the studies included in their work, so the results they reported have a lot of variability and it is difficult to draw firm conclusions on the most important compounds in the different lung diseases. In spite of this, the most promising results were found for the detection of lung cancer and for discrimination between lung cancer and other pulmonary diseases [1].

Keyword	Pubmed	Proquest
Exhaled breath condensate	805 results (106 review)	142 results (2 review)
Exhaled breath condensate and chronic obstructive pulmonary disease	13%	20%
Exhaled breath condensate and cystic fibrosis	6%	8%
Exhaled breath condensate and asthma	31%	40%
Exhaled breath condensate and lung cancer	9%	10%
Exhaled breath condensate and bronchiectasis	1,5%	3,5%
Exhaled breath condensate and sarcoidosis	1,5%	0,7%
Exhaled breath condensate and Acute Respiratory Distress Syndrome	1%	2%

Table 3. Results of the bibliometric analysis.

As to the detection of viruses DNA, there is not so much research on viral infections that cause influenza, colds and bronchitis, but EBC analysis was used to identify new viruses connected to the viral etiology of lung tumors and it may be promising for quantify viral load and for diagnose Sars-CoV-2 infection [36] [37]; in particular Khoubnasabjafari et al. [24] argue that EBC can be a promising sample for detecting nucleic acids with RT-PCR for diagnose COVID-19 infection, but this is still a hypothesis and its applicability must be tested.

However, not all researchers agree about using the EBC analysis for these purposes: Houspie et al. [38] in their research article have investigated the efficiency of virus isolation from EBC with PCR assays, compared to nasal swab virus detection, taken in parallel to validate the results; they concluded that EBC collection is not reliable to diagnose respiratory infections because they reported a viral detection rate of 7% for the EBCs, lower than the detection rate of 46.8% observed using nasal swabs; Carpagnano et al. [37], on the contrary, we were able to detect Epstein-Barr virus (EBV) and Citomegalovirus (CMV) DNA in the EBC with real-time PCR assay, two viruses which are indicative of lung cancer, if are present in the respiratory tract; the results obtained with EBC analysis have comparable sensitivity and specificity of the results obtained with the bronchial brushing fluid samples analysed with the same essay; with the EBC analysis, it was also possible to evaluate the presence of HPV DNA in the respiratory tract and the results were perfectly overlapping with that obtained from the bronchial brushing analysis [39].

All these results are highly dependent on the instrumentation used for the detection of viruses in the condensate: Gould et al. [36] affirm that Matrix-Assisted Laser Desorption Ionization Time of Flight Mass Spectrometry (MALDI-ToF-MS) is the preferred method for the identification of viral load in the condensate, because it allows to determine the unique protein profile that is characteristic of the pathogen, but the most used is PCR essay.

3.3. Biomarkers Connected to Lung Diseases

The EBC biomarkers can be divided into 3 main groups, shown in the table below (Table 4) and a single biomarker can fall into one or more of these categories [40].

Group 1	Volatile compounds (VOCs) Non-volatile compounds (non-VOCs) Non-volatile compounds derived from volatile compounds
Group 2	Very-low-molecular-weight compounds Low-molecular-weight compounds Polypeptides Proteins Nucleic acids
Group 3	Lipid mediators Inorganic molecules Organic molecules Redox relevant molecules pH relevant molecules Cytokines, chemokines

Table 4. EBC biomarker groups [40].

Among the VOCs, Nitric Oxide (NO) is the most studied and abnormalities in exhaled NO is present in several lung diseases, endogenous NO is derived from L-arginine by the enzyme NO synthase (NOS), but NO has also a non-enzymatic source; NO is produced along the entire airways and in the lower respiratory tract its concentration varies between 1 and 9 ppb. Exhaled NO increases in subjects with asthma, lung cancer and bronchiectasis, it does not change in subjects with COPD or chronic bronchitis, and it decreases in people with cystic fibrosis. [10]

Another widely studied VOCs is Carbon Monoxide (CO), mainly present in the alveoli. There are three main sources of CO in exhaled breath: enzymatic degradation of heme, non-heme-related release and exogenous CO. Its physiological concentration value is between 1 and 3 ppm, but its value increases in asthmatic subjects, with cystic fibrosis and bronchiectasis. [10]

Acetone, isoprene, and methanol are other exhaled compounds whose level changes according to the lung diseases of the patient: normal concentration of acetone is 600 ppb, in range from 177 to 2441 ppb and rise in lung cancer patient; normal concentration of isoprene is between 80 and 100 ppb, and decreases in patients with cystic fibrosis, lung cancer and asthma; normal concentration of methanol is 142 ppb, but vary from 50 to 500 ppb and it decrease in patients with lung cancer [1] [41] [42] [43].

There are proteins and lipids that are potential candidate ad markers of viral infections, in particular viral infections lead to increase the production of fatty acids, alkanes, and alkanes related products. 2,3-butandione, aldehyde, 2,8-dimethyl-undecane and n-propyl acetate have all been correlated with viral infection [36]. Cystic Fibrosis (CF) patients are often affected by a bacterial infection caused by *Pseudomonas (P.) aeruginosa*, and a VOCs profile could differentiate patients with or without this bacterial colonisation: elevated levels of exhaled sulphides and hydrogen cyanide indicate *P. aeruginosa* colonization compared to CF children without colonization [1].

Chen et al. [16] reported the VOCs biomarkers for Sars-CoV-2 infection: ethyl butyrate and isopropanol-1 rise in patient with COVID-19 in spite of healthy control; lower level of butyraldehyde, but higher level of ethyl butanoate, indicate a COVID-19 infection, higher levels of both butyraldehyde and ethyl butanoate result from infections by other pathogens, but not by SARS-CoV-2; also acetone levels for COVID-19 patients is substantially lower than those of healthy control [16].

Cytokines have been studied as possible biomarkers of lung diseases; they are small proteins divided into pro-inflammatory, anti-inflammatory cytokines and chemokines. In EBC they are identified through the ELISA assay and the cytokines IL-1 β , IL-2, IL-4, IL-5, IL-6, IL-8, IL-10, IL-17, IFN- γ , TGF- β , and TNF- α have a mean concentration of ~50 pg/mL in healthy subjects [27], but IL-6 increases in subjects with lung cancer, cystic fibrosis, COPD or asthma, IL-4 IL-8, IL-17, TNF- α increase in asthmatic subjects, IFN- γ decreases in asthmatic subjects and IL-8 is elevated in CF and COPD patients [44].

As to non-volatile biomarkers in EBC, Isoprostanes are widely studied, usually measured using enzyme immunoassays (EIA) or gas chromatography/mass spectroscopy (GC/MS); isoprostanes are produced by free-radical lipid peroxidation of arachidonic acid, and represent a marker of oxidative stress, are chemically stable and are specific for lipid peroxidation. In healthy subjects the maximum level of 8-isoprostane is 50 pg/mL, this value increases in patients with asthma, correlating with disease severity and degree of inflammation, COPD, ARDS, cystic fibrosis. [20]

Between the measurements that are carried out on the condensate, pH is the most studied as EBC biomarker [19]. In healthy subjects, EBC mean pH is 7,7, with a physiological range of 7.4–8,8, but in acute asthma, CF, COPD, bronchiectasis, and acute lung injury patients EBC pH decreases up to three log order [45].

The complete lists of VOCs and non-volatile biomarkers for lung diseases are reported in Appendix A, Table A 1 and Table A 2.

3.4. Sampling Methods

The methods of exhaled breath analysis all consist in letting the patient exhale in a collection device, with or without a condensing device, depending on the analysis to be performed on the sample. To dimension a condensing device, it is necessary to know what the normal and pathological respiratory volumes are in order to have an idea of which volumes to consider as input for the prototype, which are the collecting devices used until now and the challenges connected to the sampling collection.

3.4.1. Respiratory Volumes and Capacities

The respiratory volumes can be deduced during a spirometry and they change depending on whether the subject is healthy or pathological. The figure below (Figure 5) is a spirometric graph, that shows volumes and lung capacities, for a healthy male subject of 70

kg of weight or for a healthy female subject of 50 Kg of weight, aged 28. Details of each volume and capacity is then listed. [46]

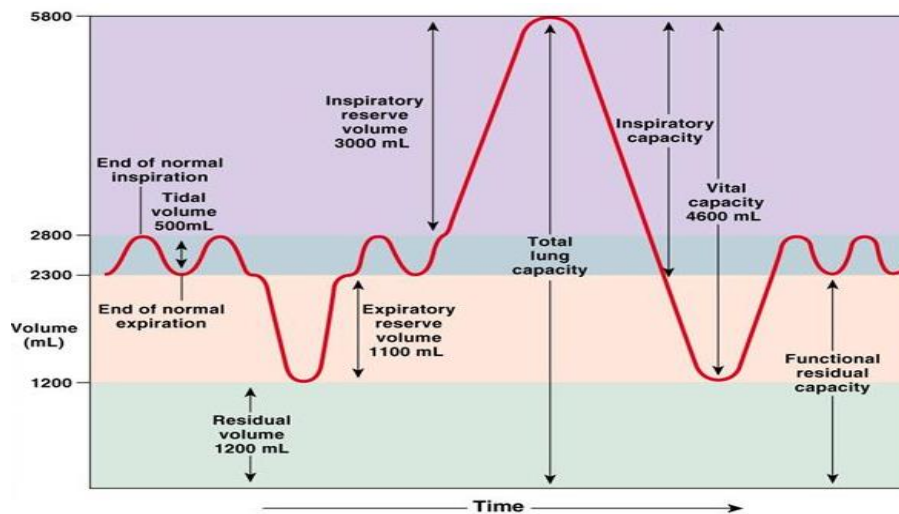


Figure 5. Spirometric graph showing lung volumes and capacities [46].

Tidal Volume (TV): air volume mobilized in each breath – 0,5 L.

Residual Volume (RV): air volume that remains in the lung at the end of a maximum exhalation – 1,2 L.

Expiratory Reserve Volume (ERV): Maximum expiratory volume since the end of normal inspiration – 1,1 L.

Inspiratory reserve volume (IRV): Maximum inspirable volume since the end of normal inspiration 3 L.

Vital Capacity (VC) or Forced Vital Capacity (FVC): maximum amount of air mobilized in a maximum breath – 4,6 L.

Total Lung Capacity (TLC): air volume presents in the lungs after a maximal inspiration of – 5,8 L.

Functional Residual Capacity (FRC): air volume present in the lungs at the end of normal breathing 2,3 L.

Inspiratory Capacity (IC): Maximum inspired air volume starting from the end expiratory volume of a normal inspiration – 3,5 L. [46]

With the spirometric test, we can calculate as well:

- The **Forced Expiratory Volume in 1 s (FEV1):** volume of air exhaled in the first second of a forced exhalation, allows to measure the emptying speed of the lungs;
- **FEV1 / FVC ratio:** ratio that allows the discrimination between an obstructive and a restrictive deficit; $0,7 < FEV1/FVC < 0,8$ are normal values or found in case of restrictive deficit, $FEV1/FVC < 0,7$ is found in case of obstructive deficit. [47]

The two most important parameters of spirometric test are FEV, FEV1 and their ratio, because they vary according to the lung

pathology [XIV]. For example, performing this test after administration of a bronchodilator the $FEV_1/FVC < 0.7$ confirms the presence of COPD and in these patients:

- Mild COPD → $FEV_1 \geq 80\%$ predicted;
- Moderate COPD → $50\% \leq FEV_1 < 80\%$ predicted;
- Severe COPD → $30\% \leq FEV_1 < 50\%$ predicted;
- Very Severe COPD → $FEV_1 < 30\%$ predicted [48].

As to cystic fibrosis $FEV_1/FVC < 0,7$ and $FEV_1 = 52-57\%$ predicted [49] and in case of asthma subjects $0,75 < FEV_1/FVC < 0,8$ in adults and $FEV_1/FVC > 0,9$ in children; in patients with moderate or severe asthma, FEV_1 increases of 13% post-bronchodilator compared to pre-bronchodilator FEV_1 [3].

A normal breathing pattern is always used to collect exhaled breath, so the EBC analysis is not affected by lung disease. The usual condenser inlet flow is 500mL/respiratory act and a healthy adult subject performs 12-20 breaths per minute [46].

3.4.2. Condensing Devices

Today there are many devices on the market to collect and condense the exhaled breath and many other experimental ones have been developed by individual research groups. Some of them are:

- ECoScreen™ I (Jaeger, Wuerzburg Germany) ECoScreen™ Turbo (VIASYS Healthcare GmbH, Hoechberg, Germany): collection systems in which exhaled air enters and leaves the chamber through a two-way valve to separate inhaled and exhaled air, they have a saliva trap and EcoVent (JAEGER, Höchberg Germany), a device to record the ventilated volumes during a tidal breath, integrated. Exhaled air flows through a lamellar condenser and an electrical refrigeration device is used to cool the expiratory air (Appendix B, Figure B 1). The interior temperature varies between -20°C and -10°C for ECoScreen™ I and is about -4°C for ECoScreen™ Turbo; [50] [51]
- RTube™ (Charlottesville, Virginia, USA): disposable and portable collection kit with a re-usable aluminium sleeve, has a mouthpiece connected through a unique one-way valve into a polypropylene collection and the circuit contains a saliva trap (Appendix B, Figure B 2) [50]. The aluminium sleeve is previously cooled at the desire temperature: the mean used temperature is -20°C [52] but some research articles reported a temperature of $-70^\circ\text{C}/-80^\circ\text{C}$ [53];
- Turbo DECCS (Medivac, Parma, Italy): portable device that consists of a disposable collection cell inserted in a peltier-

type electrical cooling system, it has a one-way valve and a saliva trap integrated (Appendix B, Figure B 3) [44]; the temperature maintained in the condensation chamber varies between -10°C and -35°C [XV];

- Modified RTube™ EBC collection apparatus: is a research-built device that consist of an EcoVent attached to the air intake end of the RTube™, connected to HEPA filter and an incentive spirometer, to help subjects normalize the volume of air during each inspiration (Appendix B, Figure B 4). The aluminium sleeve is stored in water and ice until the sample is collected and the temperature of the condensation chamber is about 4°C; [52]
- RTube™ and Loccioni instrument: is a research-built device in which the RTube™ aluminium sleeve is surrounded by dry ice within a cylindrical container, a Respirguard 303 filter (Vital Signs, San Diego, CA) is placed at the intake of the R-Tube in order to prevent the introduction of microbes and the Loccioni Instrument (Loccioni Gruppo HumanCare, Ancona, Italy) is connected at these components (Appendix B, Figure B 5). The Loccioni instrument measures CO₂ concentration, volume of each breath and total volume exhaled during sampling and has an interactive screen that visually guides the subject in the respiration; [54]
- Teflon PFA tube in ice bucket condenser system: is a self-made device that consists of an ice bucket filled with ice, in which is immersed a Teflon Perfluoroalkoxy (PFA) tube that end in a polypropylene open chamber (Appendix B, Figure B 6); there are no condensing temperature information in the research article where this collection system was used [55];
- Glass condenser system: is a self-made device that consists of an inner glass chamber, which contained ice, suspended in a larger chamber; condensate is formed on the outside surface of the inside glass that was separated from ambient air; this device has a saliva trap and a one-way valve at the outlet (Appendix B, Figure B7). There are no condensing temperature information in the research article where this collection system was used. [56]

Each exhaled air sampling device is used with different collection times or has recommended collection times different from the others; depending on this parameter, the volume of incoming air exhaled by the subject changes and consequently also the volume of EBC collected changes. In general, for all the devices mentioned above, the collection time varies from 5 to 15 minutes. [20] [52] [54] [55] [56] [57] [XV] The volume of exhaled air is approximately 105/106 L to

obtain a volume of EBC of 1 mL for the ECoScreen™ and the RTube™, for the Turbo DECCS an inlet volume of 50 L is sufficient to obtain 1,5-3 mL of condensed [52] [XV].

An important difference of these devices is the type of condensation chamber: the ECoScreen™ has a closed chamber as for the Turbo DECCS and the glass condenser system, while the RTube™ chamber, as for the Teflon PFA tube in ice bucket chamber, is open to ambient air; a closed chamber design minimizes contamination from the environmental pollutants and dust [58].

Another important difference between the exhaled air collection and condensation devices is the control over the condensation temperature: the RTube and all researcher-built devices that include the RTube in their circuit, do not have an integrated temperature control, while the ECoScreen™ and the Turbo DECCS have an electric refrigeration system, which allows to keep the temperature in the condensing chamber approximately constant. [44] [58] [XV]

A complete comparison of the collection and condensation devices of the exact breath, on the market or self-made, is reported in Appendix B, Table B1 and Table B2.

3.4.3. Sampling Challenges

The EBC analysis technique involves overcoming many challenges, some of these have already been mentioned previously, such as the lack of standardization and validation, which makes it difficult to apply these methods in clinical practice. This is directly related to the lack of reproducibility of EBC parameters across different laboratories, that decrease the comparability of EBC analysis because there are lots of sampling devices and different techniques to analyse the EBC collected. To overcome this problem, it is important to test reproducibility of each biomarker collected with various methods and to be analysed with different assays, to find the most ideal combination for best results. [20]

Contribute to problems of variability and validity of results also the fact that the levels of many EBC biomarkers are near the lower limits of assay detection, so the concentration of samples is essential for successful measure. The most promising methods of concentration are lyophilisation and solid phase extraction while ultra-filtration, freeze-drying, vacuum concentration, and concentration with pyrogallol red are found to be inapplicable. [20]

Another challenge of collecting EBC samples is sample contamination, which may be due to either ambient air or saliva or air

inhaled and exhaled from the nose [20] [45]. Ambient air contains molecules which may influence EBC composition in many ways: air components directly contribute to biomarkers levels in EBC, they react and change or consume molecules trapped in EBC, they lead to inflammatory and biochemical changes in the airway that change the EBC composition; for these reasons is fundamental to limit the contact between EBC and ambient air. As to salivary contamination, saliva contains many of the mediators that are also present in the lower airways, therefore if a little saliva contaminates the sample, the quantity of some biomarkers may change, so it is important to exclude salivary contamination; to avoid gross salivary contamination a saliva trap can be used. [45] Nasal contamination also contributes to the modification of biomarkers levels in EBC, so, during the EBC collection is better to use a nose clip, that prevents nasal inhalation and exhalation [20].

Other factors that influence the composition of the EBC and therefore make it difficult to standardize this method are: age and gender, food and drink, circadian rhythm and tobacco smoking [20]. In particular, the last one is the most important, so smokers should not smoke at least 3 h, but preferably from the evening before EBC collection to minimise its effect [45].

Chapter 4: Condensation Process Simulation in Thermodynamic Equilibrium Condition

In this chapter we will present all the analyses carried out to study the condensation process in conditions of thermodynamic equilibrium through the aspen Plus V10 software and the relative results obtained. After defining a composition profile of the exhaled air by a healthy subject and the cooling temperatures, the condensate volume, and the maximum yield of the air components as the temperature and the thermodynamic model vary was analysed, to evaluate the best one, which would match the simulation results with the data in the literature. Subsequently, we focused on ammonia, the component for which more data were found in the literature, and a sensitivity analysis was performed according to the variation of the thermodynamic model and the changes of the concentration of the other components in the exhaled air. Finally, an uncertainty budget was also performed to calculate the combined uncertainty of the simulation results, to compare the latter with the data in the literature.

4.1. Exhaled Air Composition of a Healthy Subject Used for the Simulation

The exhaled air is composed of molecular oxygen (O_2) for the 16%, 78% of molecular nitrogen (N_2), 4%-5% of carbon dioxide (CO_2), helium (He) for the 0,5%, argon (Ar) for the 0,9% and 0,9% of lots of VOCs present in traces [59] [60]. For the simulation, among the VOCs present in traces, all the previously mentioned components and collected in the Appendix A, that can be used as volatile biomarkers for lung diseases, were taken into consideration.

The relative humidity of oral exhaled air is 91%–96%, but the relative humidity of air is very variable and it can even drop to 37%, used as a reference value [59]. The psychrometric chart was used to calculate the vapour pressure (partial pressure) of water in dry air, starting from the relative humidity and the temperature; dividing the vapour pressure with the atmospheric pressure it is possible to obtain the partial pressure of water in dry air [XVI].

The percentage of water in dry air is variable, but the maximum value is around 6%, calculate with the psychrometric chart for dry-bulb $T=37^\circ C$ and $P. Atm=101325 Pa$:

- If Relative Humidity = 100% and $P. Vapour = 6306 Pa$
Molar Fraction = $(P. Vapour) / (P. Atm) = 0,062 = 6,2\%$;
- If Relative Humidity = 37% and $P. Vapour = 2333 Pa$
Molar Fraction = $(P. Vapour) / (P. Atm) = 0,023 = 2,3\%$;

- Relative Humidity = 91% and P. Vapour = 5738 Pa
Molar Fraction = (P. Vapour) / (P. Atm) = 0,057 = 5,7%. [XVI]

To analyse the condensation process, two simulations sets were performed: the first using only the elements present in greater quantities as components of the simulated exhaled air; the second using all the components, also the VOCs present in tracks.

The air composition, only for the compounds present in greater quantity, for a healthy subject expressed in molar fractions is summarized in the following table (Table 5):

Compound	Molar fractions	Reference
Water	2,3%	
Oxygen	16%	[59]
Nitrogen	76,3%	[59]
Carbon dioxide	4%	[59]
Argon	0,9%	[60]
Helium	0,5%	[59]
Tot.	100%	

Table 5. Air composition used for the simulation with the main compounds.

The complete air composition, for a healthy subject expressed in molar fractions and used for the second simulation is summarized in the following table (Table 6):

Compound	Molar fractions	Reference
Water	2,3%	
Oxygen	16%	[59]
Nitrogen	76,2994%	[59]
Carbon dioxide	4%	[59]
Argon	0,9%	[60]
Helium	0,5%	[59]
Carbon monoxide	3 ppm	[10]
Pentane	10 ppb	[1] [10]
Nitric oxide	9 ppb	[10]
Isoprene	100 ppb	[41]
Ammonia	2 ppm	[59]
Pentanal	0,27 ppb	[1]
Exanal	0,03 ppb	[1]
Octanal	0,69 ppb	[1]
Nonanal	2,38 ppb	[1]
Acetone	600 ppb	[16] [41]
Ethane	10,54 ppb	[1] [10]
Ethyl acetate	8 ppb	[1]
2-pentanone	5,1 ppb	[1]
2-propanol	4 ppb	[1]
Methanol	142 ppb	[1]

Table 6. Air composition used for the simulation with all the compounds.

As regards the aldehydes present as VOCs in the air, such as Pentanal, Hexanal, Octanal and Nonanal, values expressed in nmol/L were found in research articles in the literature. To transform them into molar fractions (mol/mol), air was considered an ideal gas as a first approximation that follows the ideal gas law and they have been multiplied by the molar volume of an ideal gas which is 24,79 L/mol in ambient standard conditions ($P=1\text{bar}$ and $T=25^\circ\text{C}=298,15\text{K}$) [31].

To set up the simulation it is also necessary to identify the gases that follow Henry's law as noncondensable components, that dissolve in a solvent and do not react and must be inserted in a special section on Aspen. This can be done using the critical temperature: if the critical temperature of this compounds is lower than the operating temperature, they are considered gases and follow Henry's law. In our simulation, the gas components are Oxygen, Nitrogen, Helium, Argon, Carbon Monoxide and Nitrogen Oxide. Noncondensable gases have a vapor pressure greater than the operating pressure at a fixed temperature, so the vapor pressure tells us whether a compound is condensable or not.

4.2. Thermodynamic Property Methods Used for Aspen Simulations

To set up a simulation in Aspen it is essential to choose the appropriate method to estimate the properties of pure compounds or mixtures because this greatly affects the simulation results; in Aspen the estimation methods are grouped in property methods and use a property method it means choose several estimation equations [32].

Aspen uses the fugacity, a physical quantity, with the dimension of a pressure, to study the transfer of matter in a multiphase system and it represents the achievement of phase equilibrium. The fugacity of i component in liquid phase for equation-of-state methods and for activity coefficient methods is:

$$f_i^V = \varphi_i^V y_i p$$

and in the vapor phase for equation-of-state methods is:

$$f_i^l = \varphi_i^l x_i p$$

and in the vapor phase for activity coefficient methods is:

$$f_i^l = x_i \gamma_i f_i^{*,l}$$

where φ_i is the fugacity coefficient, γ_i is the liquid activity coefficient of component i and $f_i^{*,l}$ is liquid fugacity of pure component i at mixture temperature.

The equilibrium is achieved when the fugacity of each component is equal in all phases:

$$f_i^V = f_i^l$$

[32] [30]

For this thesis work, the methods that well describe the liquid-vapor or liquid-liquid-vapor equilibrium were used [30]. They are listed in the table below (Table 7) and they are equation of state methods or activity coefficient methods.

Property Model	Equation of state	Activity coefficient method	Henry's law
IDEAL	Ideal gas law	-	Yes
PENG-ROB	Peng Robinson	-	No
SRK	Soave-Redlich-Kwong	-	No
NRTL	Ideal gas law	NRTL	Yes
NRTL-2	Ideal gas law	NRTL	Yes
NRTL-HOC	Hayden-O'Connell	NRTL	Yes
NRTL-NTH	Nothnagel	NRTL	Yes
NRTL-RK	Redlich-Kwong	NRTL	Yes
ELECNRTL	Redlich-Kwong	NRTL	Yes
UNIQUAC	Ideal gas law	UNIQUAC	Yes
UNIQ-2	Ideal gas law	UNIQUAC	Yes
UNIQ-HOC	Hayden-O'Connell	UNIQUAC	Yes
UNIQ-NTH	Nothnagel	UNIQUAC	Yes
UNIQ-RK	Redlich-Kwong	UNIQUAC	Yes
WILSON	Ideal gas law	WILSON	Yes
WILS-2	Ideal gas law	WILSON	Yes
WILS-HOC	Hayden-O'Connell	WILSON	Yes
WILS-NTH	Nothnagel	WILSON	Yes
WILS-RK	Redlich-Kwong	WILSON	Yes
WILS-HF	HF equation of state	WILSON	Yes
WILS-GLR	Ideal gas law	WILSON	Yes
WILS-LR	Ideal gas law	WILSON	Yes
WILS-VOL	Redlich-Kwong	WILSON	No

Table 7. Property methods used in AspenPlus [30].

The IDEAL property method assumes that the activity coefficient for the liquid phase is 1, that the vapour phase has a fugacity of 1, is based on the ideal gas law and use Rackett model for liquid molar volume estimation; this model can be used with Henry's law [32].

The PENG-ROB model uses cubic Peng-Robinson standard equation of state for all thermodynamic properties, except for liquid molar volume estimated with Rackett model for real components. It is recommended in the case of processes involving non-polar or weakly polar gases, but also for non-ideal polar chemical compounds; models the liquid-vapor equilibrium and liquid-liquid equilibrium [30].

The SRK model uses cubic Soave-Redlich-Kwong equation of state for all thermodynamic properties except for liquid molar volume evaluated with the Peneloux-Rauzy correction method for a more accurate estimation. It is recommended in the case of processes involving non-polar or weakly polar gas mixtures; models the liquid-vapor equilibrium and liquid-liquid equilibrium. [30]

As regards the activity coefficient property methods, the NRTL, UNIQUAC, WILSON models and their variances were used for simulations in this thesis work because they are all suitable for simulations with non-ideal mixtures formed by non-electrolyte and polar components, at a pressure below 10 bar [33].

The Electrolyte NRTL property method (ELECNRTL) was used for considering the electrolytic dissociation in the condensate and use the Redlich-Kwong equation of state for vapour phase properties; involves the use of Henry's law to model the solubility of supercritical gases and it is a versatile property method and can be used with any liquid electrolyte solution, from very low to very high concentrations [30].

4.3. Condensation Process Simulation Setup

For both simulation types, the one with only the main components and the one with all the components of the exhaled air, the same diagram was used on the Flowsheet, which includes a two-phase flash separator block with one material inlet and two outlets, the upper one for vapour and the lower one for liquid, as shown in the figure below (Figure 6)

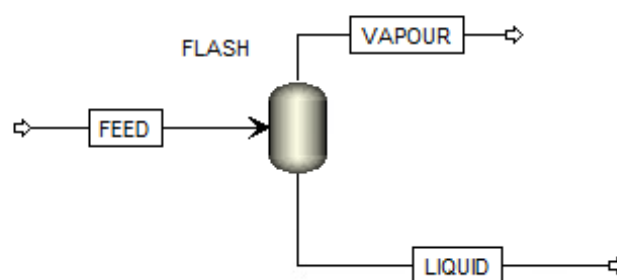


Figure 6. Diagram of a flash 2 separation in Aspen Plus flowsheet.

As regards the inlet, a temperature of 37°C, which is the typical temperature of the exhaled air, and a pressure of 101325 Pa (atmospheric pressure) were set for both types of simulations and an air flow rate of 10 L/min was chosen to simulate a person's breathing and to get to sample a volume of air of 100 L in 10 minutes, according to the data in literature.

For the flash 2 separator block an atmospheric pressure was set for both types of simulation and two phases, vapour and liquid, were considered in phase equilibrium calculations. As for the temperature reached in the separator, five different cooling temperature have been set: -4°C and -18°C temperatures easily reached by domestic refrigerators, -42°C, -80°C CO₂ dry ice temperature, -196°C liquid nitrogen temperature. As many simulations were performed.

Another simulation set was performed using a three-phase flash separator block in place of a two-phase flash separator block, to evaluate the possible formation of a further separation in the liquid phase. The three-phase flash separator block has three outlet, two liquid streams and one vapour stream and the flowsheet looks like the figure below (Figure 7)

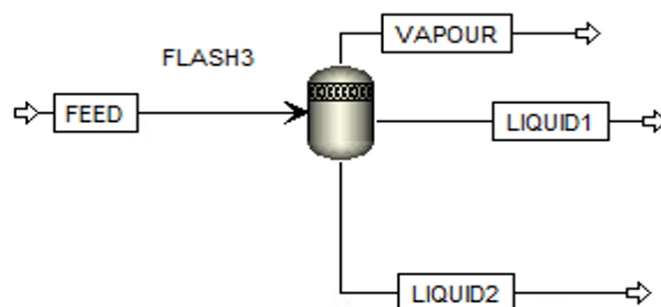


Figure 7. Diagram of a flash 3 separation in Aspen Plus flowsheet.

For the flash 3 separation block the same settings as for the flash 2 block were used.

At the end of each simulation Aspen returns a report in the form of a table, in which all the calculated properties are collected, divided by streams.

4.3.1. Aspen Sensitivity Analysis Setup

Saltelli et al. in 2004 [61] defined sensitivity analysis: “*The study of how uncertainty in the output of a model (numerical or otherwise) can be apportioned to different sources of uncertainty in the model input*”. It is used to evaluate how a dependent variable change according to the changes of an independent variable, for a given set of values for the other parameters, which remains unchanged [62].

Aspen Plus allows to perform a sensitivity analysis using the Model Analysis Tool and for this work three input variables have been changed separately in the section 'Vary' of three different Sensitivity: the FEED mole flow of Ammonia, Hexanal and Nonanal, in their range of variability in exhaled air. This analysis was carried out only for three exhaled breath components, because in the literature the range of variability of the concentration of only these components has been found both in the exhaled breath and in the exhaled breath condensate. The range of the values used for the input variables are given in the table below (Table 8):

Variable: Mole flow [mol/min]			
Component	Start point	End point	Number of points
ammonia [59]	0,02e-5	0,08e-5	3
hexanal [1]	0	1e-11	3
nonanal [1]	2,1e-10	9,6e-10	3

Table 8. Ranges and number of points of the input variables used.

In the section 'Define' of each Sensitivity, three variables were defined: the FEED mole flow the considered air component, the LIQUID mole flow of the considered air component and the volume flow of the LIQUID stream.

In the section 'Tabulate' of all the Sensitivity analyses, four variables or expressions have been inserted to be evaluated as the input variable changes his value:

- The molarity, in mol/L, of the considered component in FEED stream, obtained dividing the FEED mole flow for the input volume flow set up for the simulation;
- The molarity, in mol/L, of the considered component in LIQUID stream, obtained dividing the LIQUID mole flow for the volume flow of the LIQUID stream;
- The ratio between the molarity of the considered component in LIQUID stream, previously tabulated, and the maximum literature molarity of the same component, considered as a reference;
- The ratio between the molarity of the considered component in LIQUID stream, previously tabulated, and the minimum literature molarity of the same component, considered as a reference.

These Sensitivity Analyses were carried out changing the thermodynamic model for the simulation, while all the others simulation parameters remained unchanged and, in particular, a flash

temperature of 0°C was used for the simulation that include the sensitivity of Hexanal and Nonanal and a temperature of -20°C was set up for the simulation that include the Sensitivity of Ammonia; these temperatures are the same literature temperatures used to obtain the experimental data that were used as a reference [21] [53] [63].

Then, we focused on ammonia, as it is the component for which more data have been found in the literature, and others sensitivity analyses were carried out by varying two input variables in pairs in the 'Vary' section: the FEED mole flow of ammonia and the FEED mole flow of another component of the exhaled at a time, in their range of variability in exhaled air, to evaluate the influence of these components in the ammonia concentration in the EBC. The range of variability used for the input is given in the table below (Table 9):

Variable: Mole flow [mol/min]			
Component	Start point	End point	Number of points
Ammonia [59]	0,02e-5	0,08e-5	3
Water	9,1e-3	2,3e-2	3
Carbon monoxide [10]	3,8e-7	1,2e-6	3
Carbon dioxide [59]	1,5e-2	2e-2	3
Oxygen [59]	6,1e-2	6,3e-2	3
Nitrogen [59]	0,29	0,4	3
Pentane [1] [10]	3,9e-10	9,9e-9	3
Isoprene [41]	3,145e-8	3,94e-8	3
Nitric oxide [10]	3,9e-10	3,54e-9	3
Ethane [1]	0	4,13e-9	3
Pentanal [1]	0	1,1e-10	3
Hexanal [1]	0	1e-11	3
Octanal [1]	4e-11	2,8e-10	3
Nonanal [1]	2,1e-10	9,6e-10	3
Ethyl acetate [1]	3,9e-10	3,15e-9	3
Acetone [16] [42]	6,95e-8	5,67e-7	3
Methanol [43]	1,965e-8	1,966e-7	3
2-propanol [1]	1,179e-9	1,573e-9	3
2-pentanone [1]	3,9e-10	2,005e-9	3

Table 9. Ranges and number of points of the input variables used.

In the section 'Define' three variables were defined: the FEED mole flow of ammonia, the LIQUID mole flow of ammonia and the volume flow of the LIQUID stream.

For the section 'Tabulate' of these Sensitivity analyses, four variables or expressions were defined in the same way described above, but all of them refer only to ammonia.

A flash temperature of -20°C was used for the simulation and the property method has been varied [63], while all the others simulation parameters remained unchanged.

4.4. Uncertainty Budget Combined Uncertainty Estimation

The uncertainty budget is necessary to calculate the combined uncertainty associated with the simulated measure, the output quantity, which is a derived measure obtained as a function of other properties; these properties are called influence variables, the input quantities and their uncertainty influences the uncertainty of the output. [64]

The table (Table 10) of the uncertainty budget for combined uncertainty estimation has, as many rows as there are influence variables considered, plus a row for the results of the uncertainty estimation and the following features are tabulated by columns: name of the influence variable (i), the value of the influence variable (x_i), the uncertainty of x_i ($u(x_i)$), a function that represents the relationship between the output quantity and the influence variable ($f(x_i)$), the sensitivity coefficient ($C_i(x_i)$), the squared product of the uncertainty $u(x_i)$ and the sensitivity coefficient (k_i^2) and the significance index that is a way to identify which quantity most influences the uncertainty of the output (SI) [64].

i	x_i	$u(x_i)$	$f(x_i)$	$C_i(x_i)$	k_i^2	SI [%]
Influence variables	x_i	$u(x_i)$	$f(x_i)$	$df(x_i)/dx_i$	$(u(x_i)*C_i(x_i))^2$	$k_i^2/[\max(k_i^2)]$
Combined uncertainty	Y	$y/U(y)$			$U(y) = \sqrt{\sum_{i=0}^n k_i^2}$	

Table 10. Uncertainty budget for combined uncertainty estimation.

The function $f(x_i)$ is obtained by interpolating the experimental data obtained from a sensitivity in Aspen Plus, by varying the selected influence variable and leaving the others unchanged and the sensitivity coefficient is the partial derivative of $f(x_i)$ calculated for the fixed value of x_i .

k_i^2 represents the contributions of the uncertainty of each influence variable to the combined uncertainty of the output quantity: this is obtained calculating $U(y)$ as the square root of the sum of each contribution k_i^2 [64].

For this thesis work, a budget table to evaluate the combined uncertainty of the condensate volume obtained from the simulation and another for the combined uncertainty of the Ammonia molarity in the condensate were prepared.

4.4.1. Estimation of Condensate Volume Uncertainty

For the condensate volume combined uncertainty estimation, the following variables of influence and the relative uncertainty were chosen (Table 11):

i	x_i	$u(x_i)$
Volume [L]	100 [50] [51]	11,500
Time [min]	10 [50] [51]	0,03300
Temperature (T) [°C]	-20 [50] [51]	0,2890
Pressure (P) [Pa]	101325	57,735

Table 11. Variables of influence and the relative uncertainty for condensate volume combined uncertainty estimation.

The uncertainty related to the exhaled air volume was calculated considering a volume of air exhaled range of variation by a healthy subject of 40L, since he can perform an average of 12 to 20 breaths per minute, exhaling 0,5 L of air per breath and assuming a uniform probability distribution [46]. For this probability distribution the standard deviation is calculated as the ratio between the range of variation of the measure and square root of twelve [XVII].

As regards the uncertainty related to the sampling time, a plausible uncertainty of 2 seconds was considered and as for the estimation of temperature uncertainty, two contributions were added using the square root of the sum of squares: the first it was obtained considering a plausible variability range of measure of 1°C and a uniform probability distribution for the standard deviation calculation [XVII]; the second is the standard measuring instrument error of $4e-4$ °C [XVIII]. The uncertainty of the atmospheric pressure was estimated considering a uniform probability distribution with a variability range of 200 Pa [XIX].

4.4.2. Estimation of Uncertainty of the Ammonia Molarity in the Exhaled Breath Condensate

For the Ammonia molarity combined uncertainty estimation, the following variables of influence and the relative uncertainty were chosen (Table 12):

i	x_i	$u(x_i)$
Ammonia Molarity in input [$\mu\text{mol/L}$]	0,08 [59]	0,0173
Temperature (T) [$^{\circ}\text{C}$]	-20 [50]	11,547
Pressure (P) [Pa]	101325	57,735

Table 12. Variables of influence and the relative uncertainty for ammonia molarity combined uncertainty estimation.

The uncertainty of the Ammonia molarity entering the flash in the simulation was calculated with the square root of the sum of squares of the standard deviation of Ammonia molarity, considering a uniform probability distribution for a variability range of 0,06 $\mu\text{mol/L}$ according to the literature data [XVII] [59] and of the precision of the measuring instrument of $3\text{e-}4$ $\mu\text{mol/L}$ [65].

As regards the estimation of temperature uncertainty, two contributions were added using the square root of the sum of squares: the first it was obtained considering a variability range of measure of 40°C , according to the literature data [50] and a uniform probability distribution for standard deviation calculation [XVII]; the second is the measuring instrument error of $4\text{e-}4^{\circ}\text{C}$ [XVIII]. The uncertainty of the atmospheric pressure was the same used for the condensate volume budget.

4.5. Condensation Process Simulation Results

4.5.1. Condensate Volume Evaluation

For this work, initially the volume flow in L/min was evaluated, which multiplied by the sampling time in minutes, gave us an indication of how much condensate volume can be obtained by simulating the condensation process of the exhaled breath air. The sampling time was 10 minutes.

The simulations were performed, at the same temperature of the flash separator block, using the property methods IDEAL, PENG-ROB, SRK, NRTL, UNIQUAC and WILSON.

The condensate volume was obtained both with the simulations with only the main exhaled air compounds entering the flash, and with those with all the components; there is no variation between the two sets of simulations regarding the condensate volume, because it is composed of 99,8% water.

The results are collected in the figure below (Figure 8) and are shown in the form of mean and standard deviation of the volumes obtained as the model varies, at the same temperature because there are no significant differences in the volume of condensate obtained with the various models.

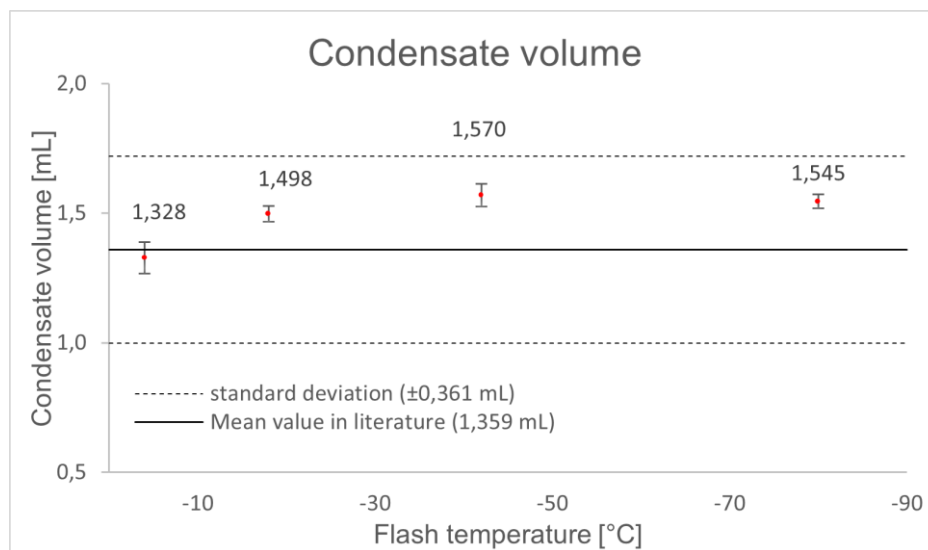


Figure 8. Condensate volume according to model and temperature variations, compared to literature data.

The figure also shows the mean value and the standard deviation of the condensate volume measurements obtained from the literature [50] [51] [52] [57]; the condensate volume is in line with this value. An exception is the case that uses a condensation temperature of -196°C , in which the condensate volume is greater ($5,713 \text{ mL} \pm 0,075 \text{ mL}$ not shown in Figure 8), but a reference was not found at this temperature, to compare the results. As the condensation temperature decreases, the condensate volume increases, as expected.

4.5.2. Yield of Every Components of Exhaled Air After Condensation Process

Subsequently, the mol flow, in mol/min, of the FEED and LIQUID streams, of each individual component in the air was considered from the report, to obtain how many moles of each of them enter the flash and how many are present in the condensate; in this way it is

possible to calculate the yield in the condensate of each single component of the exhaled air.

The results, divided by property method, are reported in the tables below (Table 13, 14, 15, 16, 17, 18, 19); nitrogen, oxygen, carbon monoxide, argon and helium have been collected in a single row of the table under the name of non-condensable gases and they have a zero yield for each temperature used.

Property method: IDEAL Sampling time: 10 minutes						
Temperature [°C]		-4	-18	-42	-80	-196
Component	Moles in exhaled air [mol]	Yield of each component				
		Flash 3 equal to flash 2				
NON-CONDENSABLE GASES	-	0%	0%	0%	0%	0%
CARBON DIOXIDE	0,16	0%	0%	0%	1%	100%
WATER	0,09	81%	94%	99%	100%	100%
AMMONIA	7,86E-06	1%	1%	4%	32%	100%
ACETONE	2,36E-06	20%	40%	79%	99%	100%
METHANOL	5,60E-07	39%	66%	94%	100%	100%
ISOPRENE	3,93E-07	8%	17%	48%	96%	100%
ETHANE	4,13E-08	0%	0%	0%	2%	100%
N-PENTANE	3,93E-08	9%	18%	50%	96%	100%
NITRIC OXIDE	3,54E-08	0%	0%	0%	0%	0%
ETHYL ACETATE	3,14E-08	43%	69%	94%	100%	100%
2-PENTANONE	2,00E-08	69%	88%	98%	100%	100%
2-PROPANOL	1,57E-08	72%	91%	99%	100%	100%
NONANAL	9,35E-09	100%	100%	100%	100%	100%
OCTANAL	2,71E-09	99%	100%	100%	100%	100%
PENTANAL	1,06E-09	66%	85%	97%	100%	100%
HEXANAL	1,20E-10	88%	96%	100%	100%	100%

Table 13. Yield of each component of exhaled air in the condensate for IDEAL property method.

Property method: PENG-ROB Sampling time: 10 minutes								
Temperature [°C]		-4	-18	-42	-80	-196		
Component	Moles in exhaled air [mol]	Yield of each component						
		One liquid phase equal for flash 2 and 3				Flash 2	Flash 3	
NITROGEN	3	0%	0%	0%	0%	0%	97%	0%
OXYGEN	0,63	0%	0%	0%	0%	0%	99%	0%
CARBON DIOXIDE	0,16	0%	0%	0%	0%	100%	100%	0%
WATER	0,09	85%	95%	100%	100%	100%	0%	100%
ARGON	0,04	0%	0%	0%	0%	0%	99%	0%
HELIUM	0,02	0%	0%	0%	0%	0%	1%	0%
CARBON MONOXIDE	1,18E-05	0%	0%	0%	0%	0%	98%	0%
AMMONIA	7,86E-06	9%	20%	61%	99%	100%	0%	100%
ACETONE	2,36E-06	0%	0%	0%	0%	100%	100%	0%
METHANOL	5,60E-07	15%	35%	81%	100%	100%	0%	100%
ISOPRENE	3,93E-07	0%	0%	0%	0%	100%	100%	0%
ETHANE	4,13E-08	0%	0%	0%	0%	37%	100%	0%
N-PENTANE	3,93E-08	0%	0%	0%	0%	100%	100%	0%
NITRIC OXIDE	3,54E-08	0%	0%	0%	0%	100%	100%	0%
ETHYL ACETATE	3,14E-08	0%	0%	0%	0%	100%	100%	0%
2-PENTANONE	2,00E-08	0%	0%	0%	0%	100%	100%	0%
2-1PROPANOL	1,57E-08	0%	0%	0%	0%	100%	100%	0%
NONANAL	9,35E-09	0%	0%	0%	0%	100%	100%	0%
OCTANAL	2,71E-09	0%	0%	0%	0%	100%	100%	0%
PENTANAL	1,06E-09	0%	0%	0%	0%	100%	100%	0%
HEXANAL	1,20E-10	0%	0%	0%	0%	100%	100%	0%

Table 14. Yield of each component of exhaled air in the condensate for PENG-ROB property method.

Property method: SRK Sampling time: 10 minutes								
Temperature [°C]		-4	-18	-42	-196	-80		
Component	Moles in exhaled air [mol]	Yield of each component						
		One liquid phase equal for flash 2 and 3				Flash 2	Flash 3	
NON-CONDENSABLE GASES	-	0%	0%	0%	0%	0%	0%	0%
CARBON DIOXIDE	0,16	0%	0%	0%	100%	0%	0%	0%
WATER	0,09	88%	96%	100%	100%	100%	0%	100%
AMMONIA	7,86E-06	0%	0%	0%	100%	1%	0%	1%
ACETONE	2,36E-06	0%	0%	0%	100%	0%	0%	0%
METHANOL	5,60E-07	1%	3%	13%	100%	85%	0%	85%
ISOPRENE	3,93E-07	0%	0%	0%	100%	0%	0%	0%
ETHANE	4,13E-08	0%	0%	0%	79%	0%	0%	0%
N-PENTANE	3,93E-08	0%	0%	0%	100%	0%	0%	0%
NITRIC OXIDE	3,54E-08	0%	0%	0%	98%	0%	0%	0%
ETHYL ACETATE	3,14E-08	0%	0%	0%	100%	0%	0%	0%
2-PENTANONE	2,00E-08	0%	0%	0%	100%	0%	0%	0%
2-1PROPANOL	1,57E-08	0%	0%	0%	100%	0%	0%	0%
NONANAL	9,35E-09	0%	0%	0%	100%	0%	38%	0%
OCTANAL	2,71E-09	0%	0%	0%	100%	0%	8%	0%
PENTANAL	1,06E-09	0%	0%	0%	100%	0%	0%	0%
HEXANAL	1,20E-10	0%	0%	0%	100%	0%	0%	0%

Table 15. Yield of each component of exhaled air in the condensate for SRK property method.

Property method: NRTL Sampling time: 10 minutes							
Temperature [°C]		-4	-18	-42	-80	-196	
Component	Moles in exhaled air [mol]	Yield of each component					
		One liquid phase for flash 3				Two liquid phases flash 3	
NON-CONDENSABLE GASES	-	0%	0%	0%	0%	0%	0%
CARBON DIOXIDE	0,16	0%	0%	0%	1%	0%	100%
WATER	0,09	81%	94%	99%	100%	100%	0%
AMMONIA	7,86E-06	57%	97%	100%	100%	100%	0%
ACETONE	2,36E-06	7%	22%	84%	100%	0%	100%
METHANOL	5,60E-07	30%	59%	93%	100%	36%	64%
ISOPRENE	3,93E-07	0%	0%	0%	0%	0%	100%
ETHANE	4,13E-08	0%	0%	0%	2%	0%	100%
N-PENTANE	3,93E-08	0%	0%	0%	1%	7%	93%
NITRIC OXIDE	3,54E-08	0%	0%	0%	0%	0%	0%
ETHYL ACETATE	3,14E-08	1%	5%	36%	99%	100%	0%
2-PENTANONE	2,00E-08	3%	12%	65%	100%	100%	0%
2-1PROPANOL	1,57E-08	35%	73%	98%	100%	100%	0%
NONANAL	9,35E-09	0%	1%	6%	100%	0%	100%
OCTANAL	2,71E-09	0%	1%	5%	98%	0%	100%
PENTANAL	1,06E-09	1%	1%	5%	59%	0%	100%
HEXANAL	1,20E-10	0%	1%	5%	80%	0%	100%

Table 16. Yield of each component of exhaled air in the condensate for NRTL property method.

Property method: UNIQUAC Sampling time: 10 minutes							
Temperature [°C]		-4	-18	-42	-80	-196	
Component	Moles in exhaled air [mol]	Yield of each component					
		One liquid phase for flash 3				Two liquid phases flash 3	
NON-CONDENSABLE GASES	-	0%	0%	0%	0%	0%	0%
CARBON DIOXIDE	0,16	0%	0%	0%	1%	27%	73%
WATER	0,09	81%	94%	99%	100%	100%	0%
AMMONIA	7,86E-06	68%	100%	100%	100%	100%	0%
ACETONE	2,36E-06	12%	42%	95%	100%	100%	0%
METHANOL	5,60E-07	30%	61%	95%	100%	6%	94%
ISOPRENE	3,93E-07	0%	0%	0%	0%	0%	100%
ETHANE	4,13E-08	0%	0%	0%	1%	19%	81%
N-PENTANE	3,93E-08	0%	0%	0%	0%	0%	100%
NITRIC OXIDE	3,54E-08	0%	0%	0%	0%	0%	0%
ETHYL ACETATE	3,14E-08	1%	5%	38%	99%	100%	0%
2-PENTANONE	2,00E-08	2%	5%	28%	96%	0%	100%
2-1PROPANOL	1,57E-08	31%	72%	99%	100%	100%	0%
NONANAL	9,35E-09	0%	1%	11%	96%	0%	100%
OCTANAL	2,71E-09	0%	1%	12%	95%	0%	100%
PENTANAL	1,06E-09	1%	2%	10%	83%	1%	99%
HEXANAL	1,20E-10	1%	2%	11%	91%	0%	100%

Table 17. Yield of each component of exhaled air in the condensate for UNIQUAC property method.

Property method: WILSON Sampling time: 10 minutes						
Temperature [°C]		-4	-18	-42	-80	-196
Component	Moles in exhaled air [mol]	Yield of each component				
		Flash 2				
NON-CONDESABLE GASES	-	0%	0%	0%	0%	0%
CARBON DIOXIDE	0,16	0%	0%	0%	1%	100%
WATER	0,09	81%	94%	99%	100%	100%
AMMONIA	7,86E-06	81%	100%	100%	100%	100%
ACETONE	2,36E-06	8%	40%	100%	100%	100%
METHANOL	5,60E-07	30%	59%	93%	100%	100%
ISOPRENE	3,93E-07	8%	17%	48%	95%	100%
ETHANE	4,13E-08	0%	0%	0%	1%	100%
N-PENTANE	3,93E-08	9%	18%	50%	96%	100%
NITRIC OXIDE	3,54E-08	0%	0%	0%	0%	0%
ETHYL ACETATE	3,14E-08	43%	69%	94%	100%	100%
2-PENTANONE	2,00E-08	69%	88%	98%	100%	100%
2-PROPANOL	1,57E-08	34%	72%	98%	100%	100%
NONANAL	9,35E-09	100%	100%	100%	100%	100%
OCTANAL	2,71E-09	99%	100%	100%	100%	100%
PENTANAL	1,06E-09	66%	85%	97%	100%	100%
HEXANAL	1,20E-10	88%	96%	100%	100%	100%

Table 18. Yield of each component of exhaled air in the condensate for WILSON property method.

Property method: ELECNRTL Sampling time: 10 minutes						
Temperature [°C]		-4	-18	-42	-80	-196
Component	Moles in exhaled air [mol]	Yield of each component				
		Flash 2				
NON-CONDESABLE GASES	-	0%	0%	0%	0%	0%
CARBON DIOXIDE	0,16	5 %	13 %	30 %	77 %	100%
WATER	0,09	84 %	96 %	100 %	100 %	100%
AMMONIA	7,86E-06	8 %	9 %	5 %	9 %	100%
ACETONE	2,36E-06	16 %	26 %	52 %	97 %	100%
METHANOL	5,60E-07	33 %	51 %	82 %	100 %	100%
ISOPRENE	3,93E-07	6 %	10 %	21 %	84 %	100%
ETHANE	4,13E-08	0%	0%	0%	0%	100%
N-PENTANE	3,93E-08	7 %	11 %	23 %	86 %	100%
NITRIC OXIDE	3,54E-08	0%	0%	0%	0%	0%
ETHYL ACETATE	3,14E-08	37 %	54 %	83 %	100 %	100%
2-PENTANONE	2,00E-08	63 %	79 %	94 %	100 %	100%
2-PROPANOL	1,57E-08	67 %	84 %	97 %	100 %	100%
NONANAL	9,35E-09	100 %	100 %	100 %	100 %	100%
OCTANAL	2,71E-09	99 %	100 %	100 %	100 %	100%
PENTANAL	1,06E-09	60 %	75 %	91 %	100 %	100%
HEXANAL	1,20E-10	85 %	93 %	98 %	100 %	100%

Table 19. Yield of each component of exhaled air in the condensate for ELECNRTL property method.

With the IDEAL (Table 13), SRK (Table 14) and PENG-ROB (Table 15) property methods, simulations were performed using both the flowsheet with flash 2 and the one with flash 3 separator block. With the NRTL (Table 16) and UNIQUAC (Table 17) models, the simulations with two-phase separator block was not performed, because these models are suitable for describing processes involving liquid-liquid separation, while with the WILSON (Table 18) property method, the simulations with flash 3 was not performed because it is not suitable for describing processes involving liquid-liquid-vapor equilibrium [33]. With the ELECNRTL (Table 19) model the simulations were performed using the flash 3 block separator.

In most of the simulated cases there is no liquid-liquid separation; a second liquid phase is formed with the use of very low temperatures: -80°C for the SRK model and -196°C for PENG-ROB, NRTL and UNIQUAC property methods. In these cases, the first liquid phase has water as a solvent, the second has carbon dioxide as a solvent.

As regards the results obtained using the PENG-ROB and SRK property method, the yield of each single component of the exhaled air is zero for temperatures above -80°C and this indicates that these two models are not satisfactory for the air condensation process the simulation. With the UNIQUAC, WILSON, ELECTNRTL and NRTL property methods it is possible to obtain a significant yield for almost all the components of the exhaled even at higher temperatures; these models and their variants were considered for subsequent analyses.

The data shown previously in the table have been collected for the ammonia, an exhaled air component also taken into consideration for subsequent analyses and in the following figure (Figure 9), the ammonia yield in the EBC as the flash temperature and the thermodynamic model vary is represented.

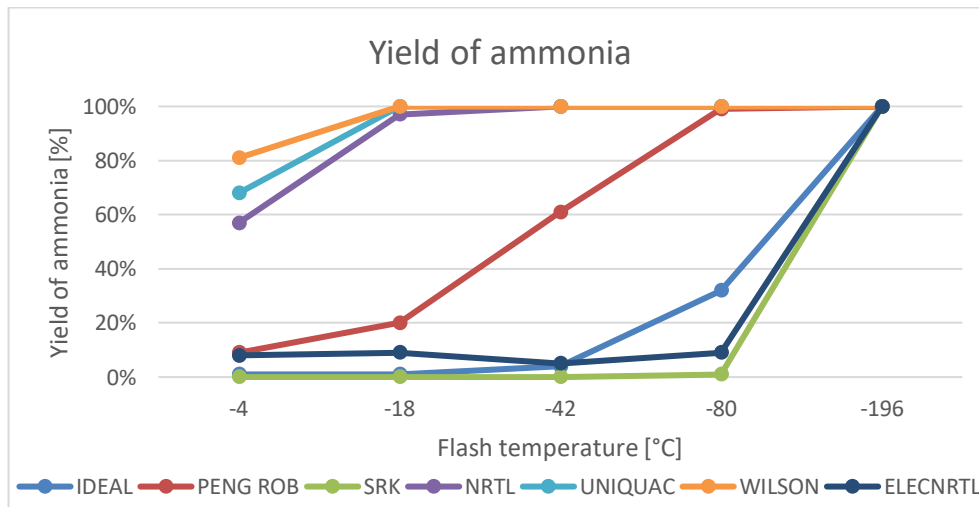


Figure 9. Yield of ammonia in the EBC.

From the graph it is noted that the ammonia yield is higher as temperatures drop, with the same thermodynamic model, but it is very variable at the same temperatures, as the model varies.

4.5.3. Sensitivity Analysis Results

To validate the results obtained from the previous analysis and to aggregate the literature data of the EBC with those concerning the exhaled air, a sensitivity analysis was performed using NRTL, UNIQUAC and WILSON models and their variants.

For each sensitivity analysis, Aspen returns a table that has as many columns as the variables or tabulated expressions inserted and as many rows as the cases considered by the software. The tables of the sensitivity analysis of Ammonia, Hexanal and Nonanal as the property method varies are shown below (Table 20, 21, 22).

The differences between the results obtained from the sensitivity analyses with the variation of the property methods were evaluated by comparing them with the coefficient of variation of the molarity data in the EBC in literature. It is calculated considering a uniform distribution of the data and is the ratio between the range of variation of the measure and square root of three multiplied by the sum of the extremes of the range [XVII]. For ammonia, this coefficient is 56%, for hexanal it is 16% and for nonanal it is 2,8%.

As regards the Ammonia sensitivity analysis results (Table 20), it is noted that there are no significant variations of the ammonia molarity in the EBC as the property method varies; the results obtained with model WILS-VOL are an exception: they are significantly different from the others and this variation is probably due to the fact that Henry's law cannot be used with this property method.

REFERENCE AMMONIA MOLARITY IN EBC = 327 [14 - 1220] [$\mu\text{mol/L}$] Flash temperature = - 20 [$^{\circ}\text{C}$] REFERENCE AMMONIA MOLARITY IN EXHALED AIR = [0,02 - 0,08] [$\mu\text{mol/L}$]				
Property method	FEED ammonia molarity [$\mu\text{mol/L}$]	Mean LIQUID ammonia molarity [$\mu\text{mol/L}$]	LIQUID ammonia molarity / max reference ammonia molarity in EBC	LIQUID ammonia molarity / min reference ammonia molarity in EBC
NRTL, NRTL-2, NRTL-NTH, NRTL-RK, NRTL-HOC	0,02	1227	1,01	87,64
	0,05	3067	2,51	219,07
	0,08	4906	4,02	350,43
UNIQUAC, UNIQ-2, UNIQ-NTH, UNIQ-RK, UNIQ-HOC	0,02	1253	1,03	89,50
	0,05	3130	2,57	223,57
	0,08	5010	4,11	357,86
WILSON, WILS-2, WILS-HF, WILS-RK, WILS-LR, WILS-NTH, WILS-GRL, WILS-HOC	0,02	1250	1,02	89,29
	0,05	3126	2,56	223,29
	0,08	5001	4,10	357,21
WILS-VOL	0,02	15	0,01	1,07
	0,05	36	0,03	2,57
	0,08	58	0,05	4,14

Table 20. Sensitivity analysis results for ammonia.

REFERENCE HEXANAL MOLARITY IN EBC = [12,7 - 22,5] [nmol/L] Flash Temperature = 0 [°C] REFERENCE HEXANAL MOLARITY IN EXHALED AIR = [0 - 0,001] [nmol/L]				
Property method	FEED hexanal molarity [nmol/L]	Mean LIQUID hexanal molarity [nmol/L]	LIQUID hexanal molarity / max reference hexanal molarity in EBC	LIQUID hexanal molarity / min reference hexanal molarity in EBC
NRTL, NRTL-2, NRTL-NTH, NRTL-RK, NRTL-HOC	0	0	0	0
	0,0005	0,113	0,005	0,009
	0,001	0,227	0,010	0,018
UNIQUAC, UNIQ-2, UNIQ-NTH, UNIQ-RK, UNIQ-HOC	0	0	0	0
	0,0005	0,155	0,007	0,012
	0,001	0,309	0,014	0,024
WILSON, WILS-2, WILS-HF, WILS-RK, WILS-LR, WILS-NTH, WILS-GRL, WILS-HOC	0	0	0	0
	0,0005	35,507	1,578	2,796
	0,001	68,791	3,057	5,417

Table 21. Sensitivity analysis results for hexanal.

As regards the results of the Hexanal sensitivity analysis (Table 21), it is noted that there are no significant changes in the ammonia molarity in EBC with the same activity coefficient method set in Aspen when the equation of state considered changes and even between the results obtained with NRTL group and UNIQUAC group of activity coefficient methods there are no significant differences. Only with the WILSON group of activity coefficient methods different results are obtained, probably due to the low hexanal concentrations in exhaled air.

With the nonanal sensitivity analysis (Table 22), similar results to those of the hexanal sensitivity analysis were obtained, with the difference that, for this component, the NRTL-HOC and UNIQ-HOC models bring significantly different results compared to those obtained with the same activity coefficient method.

REFERENCE NONANAL MOLARITY IN EBC = [17,8 - 19,6] [nmol/L] Flash temperature = 0 [°C] REFERENCE NONANAL MOLARITY IN EXHALED AIR = [0,021 - 0,096] [nmol/L]				
Property method	FEED nonanal molarity [nmol/L]	LIQUID nonanal molarity [nmol/L]	LIQUID nonanal molarity / max reference nonanal molarity in EBC	LIQUID nonanal molarity/ min reference nonanal molarity in EBC
NRTL, NRTL-2, NRTL-NTH, NRTL-RK	0,021	2,26	0,12	0,13
	0,058	6.37	0,33	0,36
	0,096	10.52	0,54	0,59
NRTL-HOC	0,021	2,1	0,11	0,12
	0,058	5,9	0,30	0,33
	0,096	9,7	0,49	0,54
UNIQUEAC, UNIQ-2, UNIQ-NTH, UNIQ-RK	0,021	3,2	0,16	0,18
	0,058	9,3	0,47	0,52
	0,096	15,2	0,78	0,85
UNIQ-HOC	0,021	2,9	0,15	0,16
	0,0585	8,2	0,42	0,46
	0,096	13,4	0,68	0,75
WILSON, WILS-2, WILS-HF, WILS-RK, WILS-LR, WILS-NTH, WILS-GRL, WILS-HOC	0,021	1676,4	85,53	94,18
	0,058	4669,9	238,26	262,35
	0,096	7663,5	390,99	430,53

Table 22. Sensitivity analysis results for nonanal.

As for these sensitivity analyses, it can be concluded that, with the same molarity in the exhaled air, its quantity in the EBC does not change significantly; this may be due to the large uncertainty and therefore variability of the data in the literature, conditioned by many factors.

As for the second group of sensitivity analyses, Aspen returns a table of results for each pair of components considered in the 'Vary' section; these have been put together in a single table of results and the percentage yield of ammonia in the condensate was calculated as the product between the ratio of volumes of condensate and air in litres and the ratio between the molarity of ammonia in the air and in the condensate in $\mu\text{mol/L}$. In the figure below (Figure 10) is shown the ammonia yield and the components that vary with ammonia are grouped three categories: water; non-condensable gases, which include oxygen, nitrogen, nitric oxide, carbon monoxide and carbon dioxide and VOCs, which include aldehydes, ketones, alcohols, alkanes, and alkenes. Within each of the groups the differences in

ammonia molarity in EBC are not significant as the second variable component changes, they are below the coefficient of variation of ammonia data in literature, which is equal to 56%.

For this analysis, the NRTL-RK and ELECNRTL property methods were used; the results obtained with the two models are the same and this indicates that there is no electrolytic dissociation in the condensate.

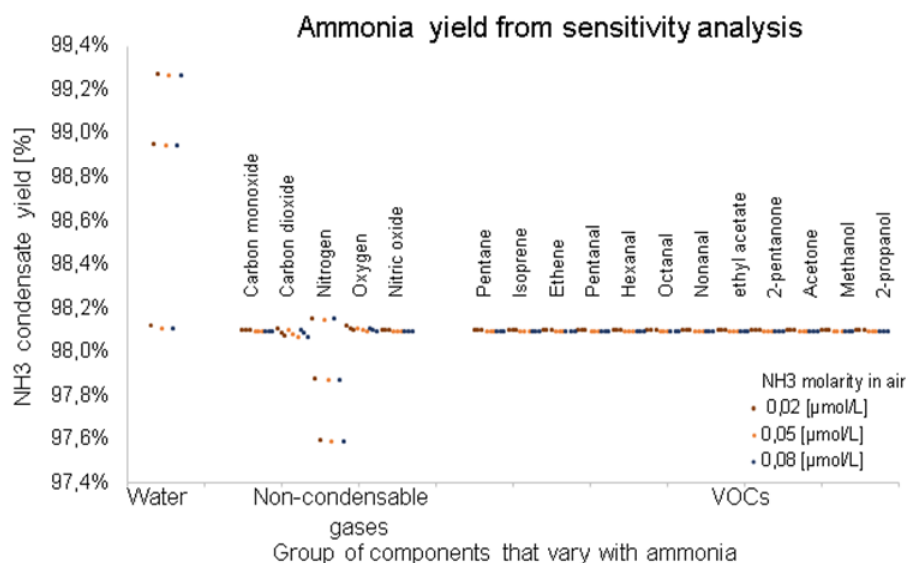


Figure 10. Yield of ammonia in the condensate.

From these sensitivity analyses, it can be concluded that, the yield of ammonia in the EBC does not change significantly when the second component considered varies. This can also be seen from the figure (Figure 11) below, which shows the deviation of the ammonia yield from the average yield value of ammonia in EBC.

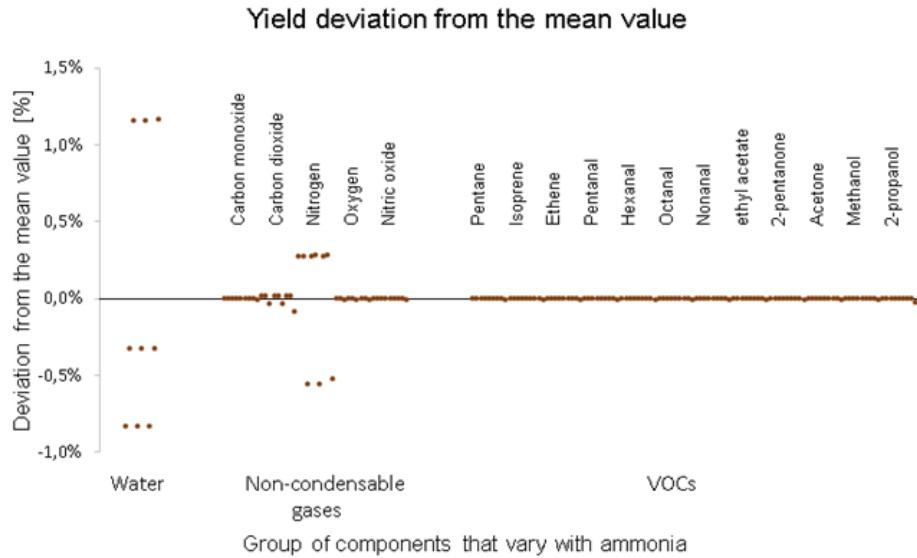


Figure 11. Yield deviation from the mean value of ammonia yield in EBC.

4.5.4. Results of Uncertainty Budget

To compare the literature data of the condensate volume and the Ammonia molarity in EBC with the results obtained from the simulation, a table was compiled with the uncertainty budget and the NRTL-RK thermodynamic model was chosen to carry out these analyses.

The uncertainty budget table for the EBC volume is shown below (Table 23):

i	x_i	$u(x_i)$	$f(x_i)$	$C_i(x_i)$	k_i^2	SI [%]
Volume [L]	100	11,5	$y = 0,0016x_i - 1E-11$	0,0016	3,413E-4	0%
Time [min]	10	0,033	$y = 1,5562x_i^{-1}$	-1400,6	2179,583	100%
Temp [°C]	-20	0,289	$y = -3E-7x_i^3 - 4E-5x_i^2 - 0,0021x_i + 0,1265$	-0,0021	3,756E-7	0%
Pressure [Pa]	101325	57,735	$y = 1E-7x_i + 0,1457$	1E-07	3,333E-11	0%
EBC volume [mL] (y)	1,557	0,0333			46,686	

Table 23. Uncertainty budget for combined uncertainty estimation of EBC volume.

This result was compared with the EBC volume in literature (Figure 12): Soyer et al. [50] affirm that, using the RTube collection device, a condensate volume of $1,51\text{ml} \pm 0,09\text{ml}$ was obtained for a sampling time of ten minutes during tidal breathing of healthy subjects and, similarly Hüttmann et al. [51] in their research article collected a condensate volume of $1,405\text{ml} \pm 0,082\text{ml}$ with the RTube in the same condition of the previous study.

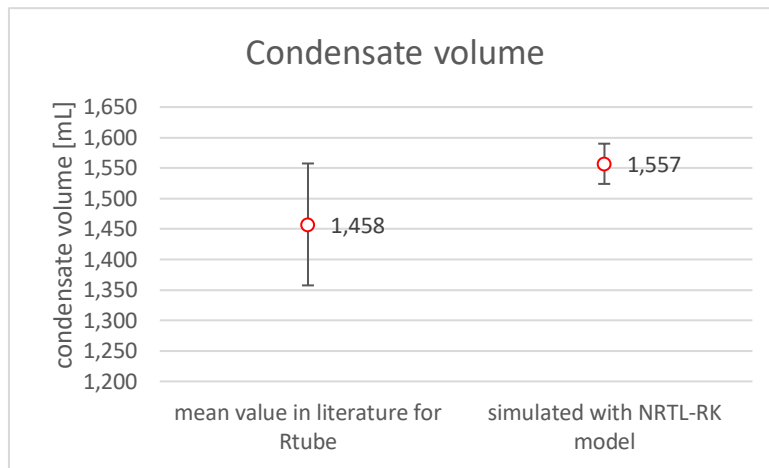


Figure 12. Comparison between the literature data of the condensate volume with the simulation data.

From the previous figure it is noted that the condensate volume obtained from the Aspen simulations and that obtained from the literature are not significantly different.

The uncertainty budget table for the Ammonia molarity in EBC is shown below (Table 24):

i	x_i	$u(x_i)$	$f(x_i)$	$C_i(x_i)$	k_i^2	SI[%]
Ammonia molarity in air [$\mu\text{mol/L}$]	0,08	0,0173	$y = 62986x_i + 1,6801$	62986	1190458,09	100%
Temp [$^{\circ}\text{C}$]	-20	11,547	$y = 4E-5x_i^5 + 0,0049x_i^4 + 0,1754x_i^3 - 2,0063x_i^2 - 190,58x_i + 2770,2$	-24,6	81003,187	7%
Pressure [Pa]	101325	57,735	$y = -0,0022x_i + 5264,1$	-0,0022	0,016	0%
Ammonia molarity in EBC [$\mu\text{mol/L}$] (y)	4954,4	4,3938			1127,59	

Table 24. Uncertainty budget for combined uncertainty estimation of ammonia molarity in EBC.

This result was compared with the ammonia molarity in EBC in literature (Figure 13): the mean value is 603 [$\mu\text{mol/L}$] according to Hunt et al. [63] research article and the uncertainty was calculated considering a linear distribution, knowing from the literature data that the range of variability is between 14 and 1220 [$\mu\text{mol/L}$] [45] [63].

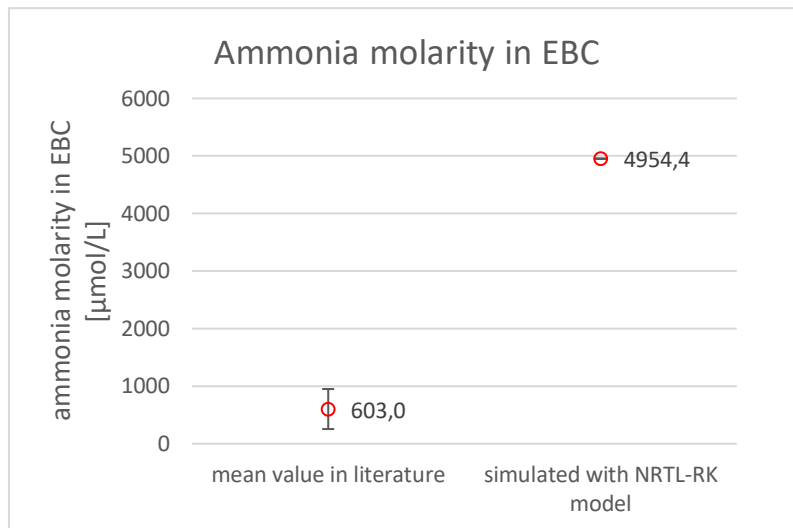


Figure 13. Comparison between the literature data of the ammonia molarity in EBC with the simulation data.

From the figure above it is noted that the ammonia molarity in EBC obtained from the Aspen simulations and that obtained from the literature are significantly different.

Chapter 5: Condensation Process Simulation in Real Condition: CFD Simulation

In this chapter it is presented the simulation of the condensation process in similar to reality conditions, to evaluate with which heat exchange area we are close to the thermodynamic equilibrium, the ANSYS software was chosen to perform a CFD simulation.

ANSYS is equipped with a worksheet called workbench in which it is possible to create a scheme of all the phases that a CFD simulation needs, as shown in the Figure 14. Each phase is linked to a subroutine which can be accessed with a suitable software.

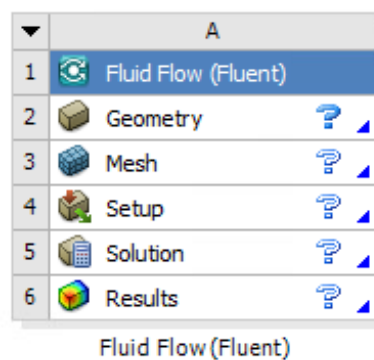


Figure 14. Design scheme for a Fluent CFD simulation.

To start performing a series of CFD simulations it is necessary to define the geometry of the condenser and the mesh to be imported in Fluent; a 3D cylindrical solid was chosen for the simulations because on the cylinder wall we expect the formation of the condensate film and its consequent precipitation by gravity. This was designed in Ansys Space Claim, a 3D CAD modelling software.

The 3D geometry was then imported into ANSYS Fluent Meshing and the surfaces were renamed to distinguish the inlet, the outlet, the wall of the cylinder, and the area where the fluid will flow (Fluid domain). In the figure below is reported the longitudinal section of the cylinder (Figure 15).

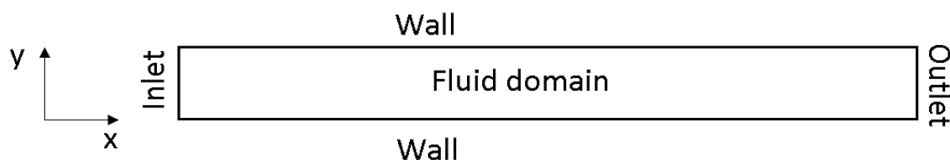


Figure 15. longitudinal section of the cylinder with named parts.

It was also created a mesh of this geometry and it was imported in ANSYS Fluent for the CDF simulation.

5.1. Simulation of Condensation Process in Literature

To start performing a simulation of the condensation process, it was used an air-water system to evaluate the simulation conditions and the first problems found. Many research groups have modelled the condensation equilibrium, but for their studies, they have used user-defined functions (UDF), that are user-written function codes, that can be loaded to enhance the standard features of Fluent's code.

Yi Qiuji et al. [66] have studied the condensation of water vapor with air as the non-condensable gas on an isothermal vertical plate, using the two phases Volume of Fluid (VOF) model, available in Fluent. They carried out a two-dimensional steady state analysis, modelling both the gas mixture region and the liquid film; the water vapor and the air mixture was introduced at the inlet with a given mass flow rate, temperature and mass fraction of the water vapor. All the thermal properties of the fluids materials were assumed to be functions of temperature and were calculated in user defined functions (UDF); mass source term, energy source term and species source term were also calculated using UDF, in order to efficiently model the wall condensation. Yi Qiuji research group have used the velocity inlet boundary condition for the vapor-gas inlet and the outlet is selected as the pressure outlet boundary, while the wall is taken as isotherm wall boundary and the other side is selected as the symmetry boundary [66].

The research group of Yoon et al. [67] also studied the film condensation of steam with noncondensable gas on a flat surface modelling the mass transfer between phases with a UDF, because they think that the standard models can be unreliable for general filmwise condensation phenomena. They used a single-phase approach, that is convenient as it avoids the need to model two-fluid problems and mathematical complications arising from the two-phase simulations; they considered only filmwise condensation, but the computational domain only includes gas mixture, formed by air and water vapour, and the condensate film layer is not explicitly modelled. Typically, when this simplification is done, the condensing boundary is treated as a dry no-slip wall, which it is not physically accurate, because the condensing layer is the liquid-gas interface, but these researchers of the University of Wisconsin incorporate the characteristics of liquid-gas interface in the condensing surface modelling it as a free surface, that is a boundary with zero shear stress in all directions. [67]

Sun D. et al. [68] are interested in model the evaporation and condensation phase-change problems with Fluent and they improve

the accuracy of the standard Volume of Fluid (VOF) method, that cannot simulate well the heat and mass transfer through the phase interface, building a new phase-change model code using UDFs. This method is suitable for incompressible, laminar, and unsteady two-phase flow and heat transfer problems. The UDFs that this group of researchers wrote allow to calculate the interfacial mass transfer flux of the vapour and of the liquid phases (\dot{m}_l and \dot{m}_v) and the heat source term (S_h) for the case in which one phase is unsaturated and the other is saturated and the thermal conductivity of the saturated phase is assumed equal to that of the unsaturated phase.

From these articles it is clear that modelling the condensation process is very complex and requires the addition of pieces of balance equations through the UDFs, but writing and inserting them is a laborious process and debugging is also very time consuming. For this reason, the simulation model that will be presented in the following paragraphs does not have the insertion of UDFs, unlike the cases reported in the literature, so it will not have the best performance ever, but represents a compromise between system complexity and precision of the results.

5.2. CFD Simulation with Small Dimension Geometry

In this thesis work, as a first attempt to approach the problem of fluid dynamics simulation of the condensation process, a geometric model, smaller than the real size, discretized with a mesh of few elements, was used. This first simulation was used to obtain the feasibility results of the condensation CFD model, despite the small size of the cylinder brings the fluid into a transition motion regime.

5.2.1. Geometric Model and Mesh

In Ansys Space Claim, a 2D geometry of a circle, with a diameter of 1 cm, was drawn in the z-y plane and was extruded in the positive direction of the x axis to obtain a cylinder of 5 cm of length. The cylinder wall has an area of 15,69 [cm²], which is the heat exchange area.

The mesh was created with the tetrahedrons method and a max face size of 1 mm. Since the formation of the film on the cylinder wall is expected, the mesh was thickened in this area using the inflation function, setting 'smooth transition' as inflation option and '10' as maximum numbers of layers. The mesh looks like in the figure below (Figure 16).

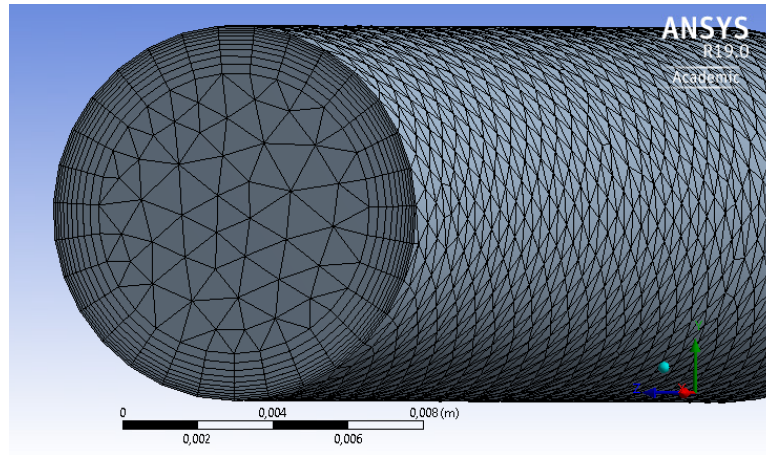


Figure 16. Mesh of the small dimension geometry.

The characteristics of this mesh are collected in the table below (Table 25):

N° of elements	N° of nodes	Skewness	Orthogonality
51223	22549	0,177±0,125	0,81±0,12

Table 25. Characteristics of the small cylinder mesh.

5.2.2. CFD Simulation Setup in ANSYS Fluent

For the general setup of Fluent, the steady option was chosen with an acceleration of gravity equal to -9.81 m/s^2 along the y axis.

The settings of the 'Models' section are summarized in the table below (Table 26):

Multiphase	Energy	Viscous	Species
Volume of Fluid Two phases	On	K-epsilon Enhanced wall treatment Thermal effects Viscous heating	Species transport
Heat exchanger	Discrete Phase	Solidification/melting	Eulerian wall film
Off	Off	On	On

Table 26. Settings for 'Models' section of Fluent.

Since the diameter of the tube is very small, with the mass flow rate set at the inlet, the flow rate is not laminar, but in transition regime; for this reason, the viscous k-epsilon model was set.

The solidification/melting model was activated because ice formation is expected as temperatures below the solidification temperature of the water in the condenser are reached and the Eulerian Wall Film was activated because is expected the formation of water liquid film.

As for the materials, phase two is formed by a mixture of air and water vapor and phase one is formed by liquid water. Phase two in inlet is made up of 2.3% of water vapor and, the remaining part is air, in molar fractions, as was also set in Aspen; in outlet the phase two is formed by 0.1% of water vapor.

In the phase interaction section, it was also set a mass transfer mechanism between the water vapour in the phase one and the liquid water of the phase two. The evaporation-condensation mechanism was chosen, with the saturation temperature that varies in a linear way with the pressure. This mechanism is based on the phase-change model proposed by Lee, that affirms that the mass transfer follows the two equations below, the first for the evaporation process and the second for the condensation process:

$$\dot{m}_v = -\dot{m}_l = r\alpha_l\rho_l \frac{T - T_{sat}}{T_{sat}} \quad T > T_{sat}$$

$$\dot{m}_l = -\dot{m}_v = r\alpha_v\rho_v \frac{T_{sat} - T}{T_{sat}} \quad T < T_{sat}$$

\dot{m} = interfacial mass transfer flux for liquid and vapour phase [Kg/m³ s]

α = volume fraction

ρ = density [Kg/m³]

r = mass transfer intensity factor [1/s] (empirical coefficient)

T = operative temperature [K]

T_{sat} = saturated temperature [K]

[68]

As regards the boundary conditions, they have been set as summarized in the table below (Table 27):

Boundary condition				
Zone	Type	Characteristics	Phase 2	Phase 1
Inlet	Mass flow inlet	Temperature: 310,15 [K] Pressure: 111325 [Pa]	Mass flow rate: 0,0002 [Kg/s]	Mass flow rate: 0 [Kg/s]
Outlet	Pressure outlet	Temperature: 298,15 [K] Pressure: 101325 [Pa]	-	-
Wall	Wall	Stationary wall, no slip Temperature: 253,15 [K] Initial Wall Film Temperature: 253,15 [K]	-	-
Fluid domain	Interior	-	-	-

Table 27. Settings for the boundary conditions.

A pressure of 111325 [Pa] has been set in inlet, because the maximum exhalation pressure is 10000 [Pa], as reported in literature [69], in addition to the atmospheric pressure of 101325 [Pa].

After initialization with initial values compute from inlet, the simulation was performed with the solution method 'coupled' and the residuals were set as default with a value of $1e-6$ for Energy equation and $1e-3$ for the other equations. The 'automatic' time step method was used.

5.3. CFD Simulation with Real Dimension Geometry

After verifying the feasibility of the CFD simulation setting for condensation with a reduced geometry, the cylinder size was increased to the realistic size. The chosen size is similar to the size of the RTube™ [XX].

5.3.1. Geometric Model and Meshing

In Ansys Space Claim, a 2D geometry of a circle, with a diameter of 4 cm, was drawn in the z-y plane and was extruded in the positive direction of the x axis to obtain a cylinder of 25 cm of length. The cylinder wall has an area of $314,1 \text{ [cm}^2\text{]}$, which is the heat exchange area.

The mesh of this geometry was created using sweep method with a max face size of 7 mm and sweep element size of 7 mm. This method has been chosen as it is more suitable for the discretization of a cylinder: it allows to have hexahedral elements with the faces arranged perpendicular to the direction of the fluid flow. The Size Facing option was used to thicken the mesh on the wall, where condensate is expected to form.

The mesh looks like in the figure below (Figure 17).

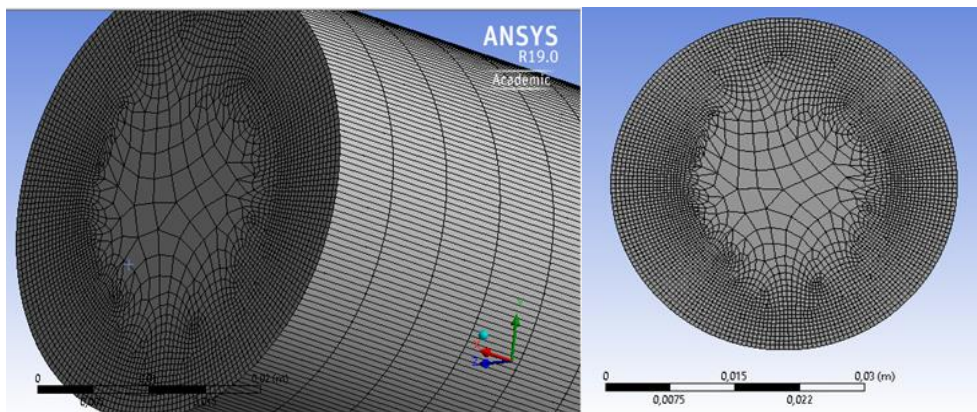


Figure 17. Mesh of the cylinder.

Later, the diameter of the cylinder was reduced of the 25% and it went from 4 [cm] to 3 [cm]. The area of the cooled wall of the cylinder went from $314,1 \text{ [cm}^2\text{]}$ to $235,6 \text{ [cm}^2\text{]}$. This geometry was discretized with elements of the size chosen during the mesh validation process described in the next paragraph.

5.3.2. Mesh Verification and Validation

The V&V (Verification and validation) guides [70] affirms:

“Verification is the assessment of the accuracy of the solution to a computational model by comparison with known solutions.

Validation is the assessment of the accuracy of a computational simulation by comparison with experimental data.”

There are many methods to verify a CFD simulation mesh. In the case of simulation of the condensation process with a cylindrical geometry, performed in this thesis work, it is possible to perform an energy balance for the chosen geometry and compare the expected theoretical results, obtained from the mathematical model, with the ones of the fluid dynamics simulation. It is possible to evaluate the inlet and outlet temperatures in Fluent and compare them with those of the mathematical model.

An operational method to validate the mesh consists in evaluating the stability of the results when the mesh changes for the same geometry, that is evaluate how the value of some output parameters varies as the mesh varies. In this thesis work, two reference parameters were chosen to validate the mesh: the volume of condensate obtained and the mean temperature of a cylinder section at a certain distance from the inlet.

The mesh generated to evaluate these parameters differ in the maximum element size in Size Facing, that is, they have the area close to the wall of the cylinder progressively discretized with smaller elements.

The characteristics of these mesh are collected in the table below (Table 28):

Characteristic	Mesh 1	Mesh 2	Mesh 3	Mesh 4	Mesh 5	Mesh 6
Element size in face sizing	0,3 [mm]	0,1 [mm]	0,08 [mm]	0,05 [mm]	0,03 [mm]	0,01 [mm]
N° of elements	160992	258048	271188	307836	314676	465912
N° of nodes	168757	270692	284345	322862	329929	485995
Skewness	0,075± 0,120	0,084± 0,135	0,074± 0,106	0,082± 0,136	0,083± 0,128	0,067± 0,139
Orthogonality	0,98± 0,06	0,97± 0,08	0,98± 0,05	0,97± 0,08	0,98± 0,07	0,97± 0,08

Table 28. Characteristics of the mesh.

As regard the reference parameters considered, the condensate volume obtained in the tube, gives us a quantitative measure on the well working of the simulations and allows us to perform a validation

with previous results of simulations in Aspen; evaluating it as the mesh changes reduces the uncertainty related to the calculation of this parameter and shows us if the separation and condensation mechanisms are working well and therefore if the phase-exchange mechanisms in the cylinder change with the mesh.

The temperature in a section of the cylinder, on the other hand, gives us an indication of the heat subtracted in that section to the fluid and therefore it is an index of the heat exchange mechanism; evaluating it as the mesh varies makes us understand if the heat exchange always achieves the same result.

The pseudo time step value, for which the simulation reaches convergence, was also evaluated; this parameter gives us an indication of the performance of the simulation.

5.3.3. CFD Simulation Setup in ANSYS Fluent

With the validated mesh, two set of simulations were carried out, changing the wall temperature in the boundary conditions. For these, the same settings from the previous simulation were used, except those listed in the following table (Table 29), which have been changed.

Setting	First set of simulations	Second set of simulations
Viscous	Laminar	Laminar
Solidification/ Melting	Off	Off
Phase 2 material in outlet	0,1% water liquid	0,8% water liquid
Inlet boundary condition	Velocity inlet Velocity: 0,132 [m/s] Pressure: 111325 [Pa] Phase 2 volume fraction: 1	Velocity inlet Velocity: 0,132 [m/s] Pressure: 111325 [Pa] Phase 2 volume fraction: 1
Wall boundary condition	Temperature: 253,15 [K] Initial Wall Film Temperature: 273,15 [K]	Temperature: 277,15 [K] Initial Wall Film Temperature: 277,15 [K]
Outlet boundary condition	Temperature: 273,15 [K]	Temperature: 277,15 [K]

Table 29. Changes in CFD simulation setting.

As regards the flow regime, the Laminar model was activated because the Reynolds numbers, calculated for humid air flowing in a circular tube, are below 2000.

Initially only the temperature of -20°C was used for the wall with the solidification/melting model activated, but the simulation did not reach convergence, so the solidification/melting model was deactivated to reduce the computational time and, consequently, the Initial Wall Temperature have also been increased to prevent by force the

formation of solid phase in the cylinder. later the wall temperature was also increased to 4°C, because at these temperatures there is no solidification of the condensate.

The simulation was performed with the solution method 'coupled' and the default values (1e-6 for Energy equation and 1e-3 for the others) were used for the residuals. The 'user specified' time step method was set with a pseudo time step that starts from the value of 1e-3 and is progressively halved until the simulation reaches convergence; at the same time, the pseudo time step in the section of the Eulerian Wall Film was also modified with the same value.

Two more simulations were performed with the same settings as the previous but with the geometry with the reduced diameter. After this modification, the inlet speed of phase 2 was also increased to keep the flow rate fixed.

5.4. Results of CFD Simulation in ANSYS Fluent

As for the results of the CFD simulations, is expected the condensate to start forming on the cylinder wall, which is the coldest area and then to precipitate by gravity and to accumulate in the lower part of the cylinder; is also expected that, in quantity, the results are in line with those obtained from the simulations in Aspen.

5.4.1. Results of CFD Simulation with Small Dimension Geometry

The CFD simulation with the small geometry converges and in the cylinder 2,3e-4 [mL] of condensate were obtained. The figure (Figure 18) below shows the volume fraction of the phase 1, the liquid phase, and it is evident that condensate forms on the cylinder wall but not evenly.

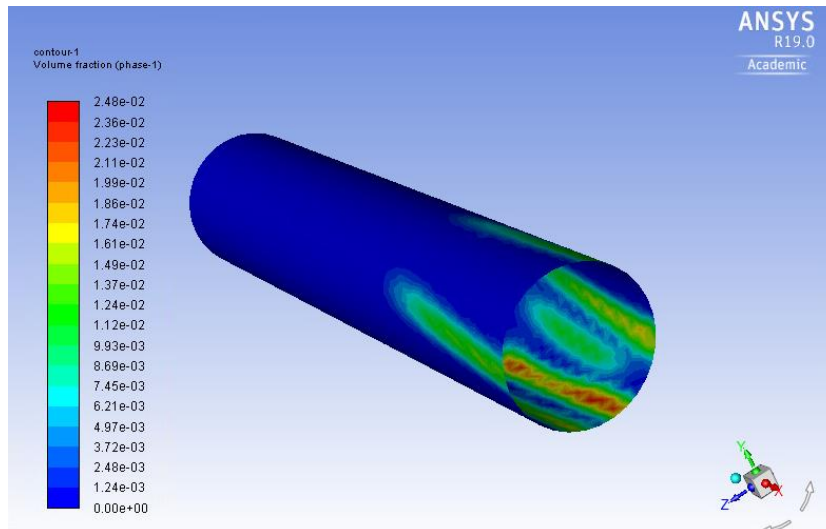


Figure 18. Contour of the phase 1 volume fraction on the cylinder wall.

The figure (Figure 19) below, instead, shows the distribution of temperatures in a longitudinal section of the cylinder.

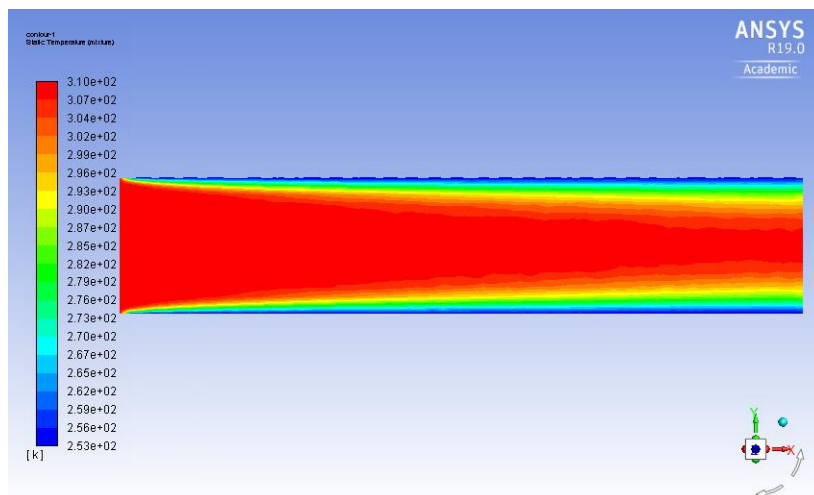


Figure 19. Contour of the temperature in a longitudinal section of the cylinder.

5.4.2. Results of Mesh Validation

The results of the analyses carried out to verify and validate the meshes are reported in the tables below (Table 30, 31). At the same wall temperature, the simulations converge with the same pseudo time step value as the mesh changes. The mean temperature was calculated in a section of the cylinder at 20 [cm] from the inlet.

Wall temperature: -20°C						
Parameter	Mesh 1	Mesh 2	Mesh 3	Mesh 4	Mesh 5	Mesh 6
Condensate volume [mL]	2,8	2,8	3,2	3,2	2,6	3,2
Mean temperature in a section [K]	279,10	286,61	291,00	284,28	284,53	287,91
Min pseudo time step [s]	1e-6	1e-6	1e-6	1e-6	1e-6	1e-6

Table 30. Parameters evaluated for the mesh (Wall temperature = -20°C).

Wall temperature: 4°C						
Parameter	Mesh 1	Mesh 2	Mesh 3	Mesh 4	Mesh 5	Mesh 6
Condensate volume [mL]	1,7	2,1	1,9	2,4	2,2	2
Mean temperature in a section [K]	288,80	285,46	289,69	288,37	292,08	291,35
Min pseudo time step [s]	5e-6	5e-6	5e-6	5e-6	5e-6	5e-6

Table 31. Parameters evaluated for the mesh (Wall temperature = 4°C).

The two parameters of interest have been reported in the following graph (Figure 20) in relation to the mesh, identified by the number of elements from which it is composed, for the two wall temperatures for which it was tested.

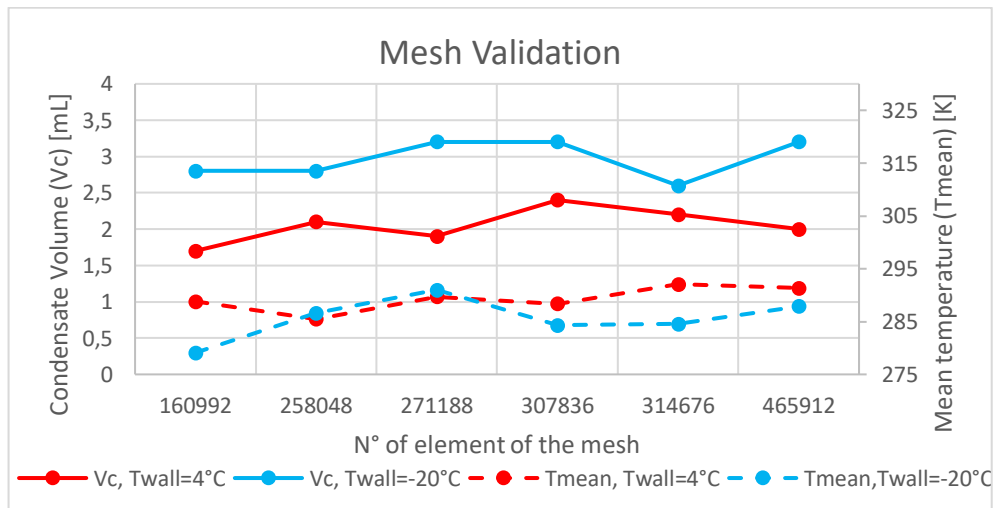


Figure 20. parameters of validation for each mesh.

There are little differences in the results obtained between the mesh 5 and 6, therefore, we can conclude the grid dependence is acceptable, and the mesh 5 is validated and used in the following simulations.

5.4.3. Results of CFD Simulation with Real Dimension Geometry

As regards the CFD simulation with the real dimension geometry and -20°C as wall temperature, in the cylinder 2,6 [mL] of condensate were obtained. The figure (Figure 21) below shows the volume fraction of the phase 1, the liquid phase, in a longitudinal section of the cylinder, in the inlet end outlet areas and in a section of the cylinder 20 [cm] away from the inlet. The condensate accumulates in the lower part of the cylinder but does not form a film on the cylinder wall.

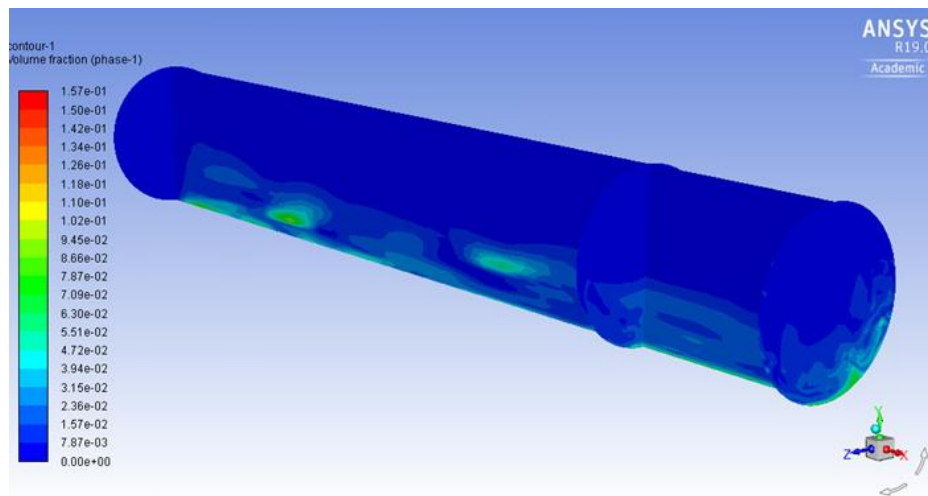


Figure 21. Contour of the phase 1 volume fraction (Wall temperature = -20°C).

The figure (Figure 22) below shows the distribution of temperatures in a longitudinal section of the cylinder, in the inlet end outlet areas and in a section of the cylinder 20 [cm] away from the inlet.

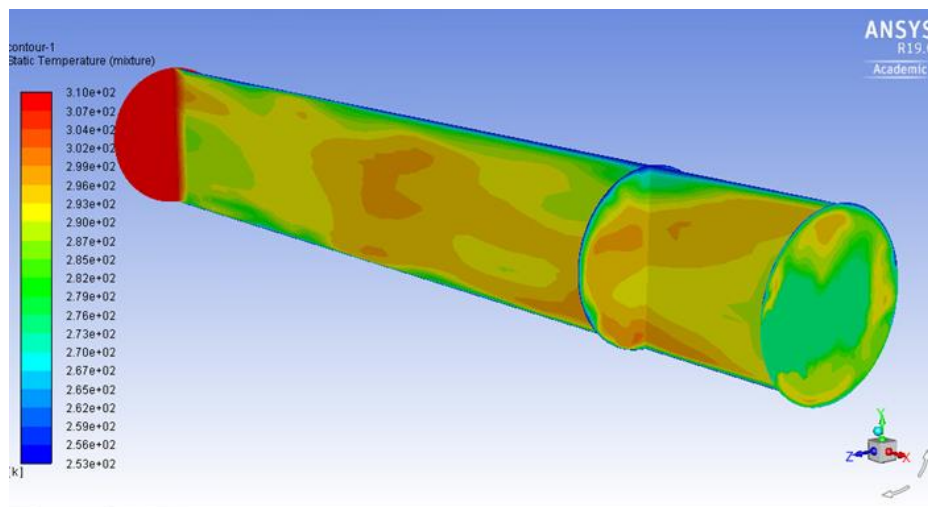


Figure 22. Contour of the temperature (Wall temperature = -20°C).

As regards the CFD simulation with the real dimension geometry and 4°C as wall temperature, in the cylinder 2,2 [mL] of condensate were obtained. The figure (Figure 23) below shows the volume fraction of the liquid phase, that, as in the former simulation accumulates in the lower part of the cylinder.

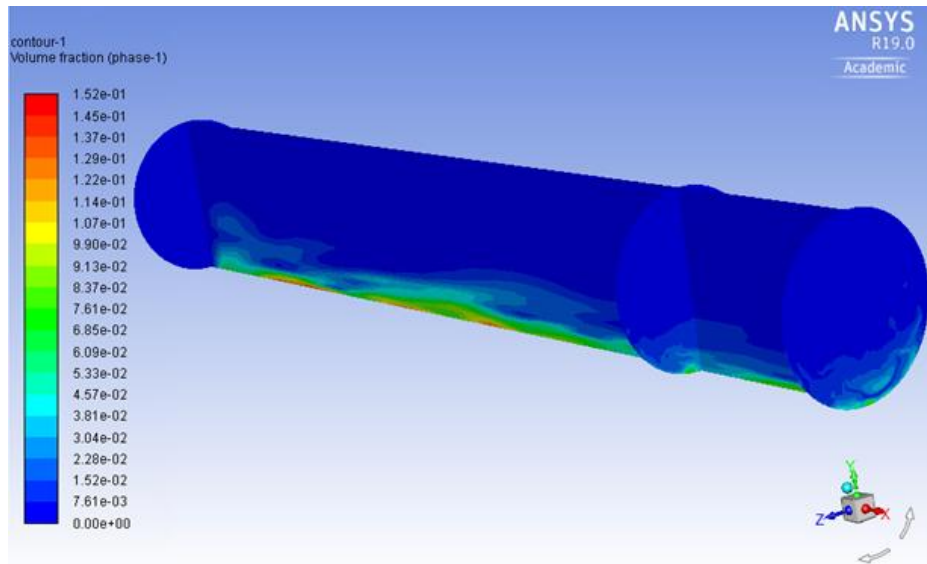


Figure 23. Contour of the phase 1 volume fraction (Wall temperature = 4°C).

The figure (Figure 24) below shows the distribution of temperatures in a longitudinal section of the cylinder, in the inlet end outlet areas and in a section of the cylinder 20 [cm] away from the inlet.

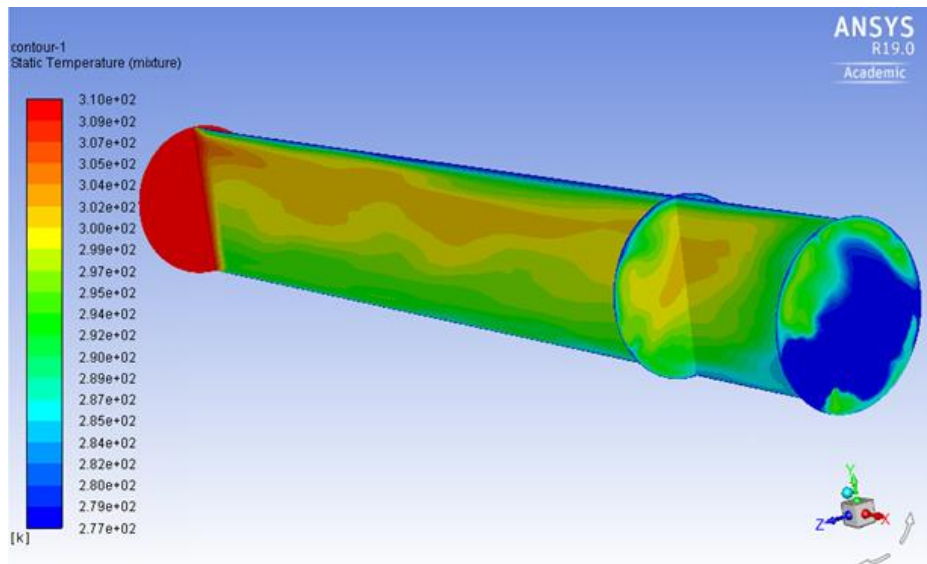


Figure 24. Contour of the temperature (Wall temperature = 4°C).

Similar contours were also obtained for the simulations with the reduced cylinder diameter.

The variations in the volume of condensate obtained for the various simulations have been reported in the following graph (Figure 25), as

the area of heat exchange varies, therefore the area of the cylinder wall.

The heat exchange areas of the two cylinder with different diameters, used in the simulations are reported in the table (Table 32) below and are related to the length of the tube, calculated as distance from the inlet section.

Distance from the inlet [cm]	Heat exchange area [cm ²]	
	D = 4 [cm]	D = 3 [cm]
5	62,82	47,12
10	125,64	94,25
15	188,46	141,36
20	251,28	188,48
25	314,10	235,60

Table 32. Heat exchange areas related to the cylinder length.

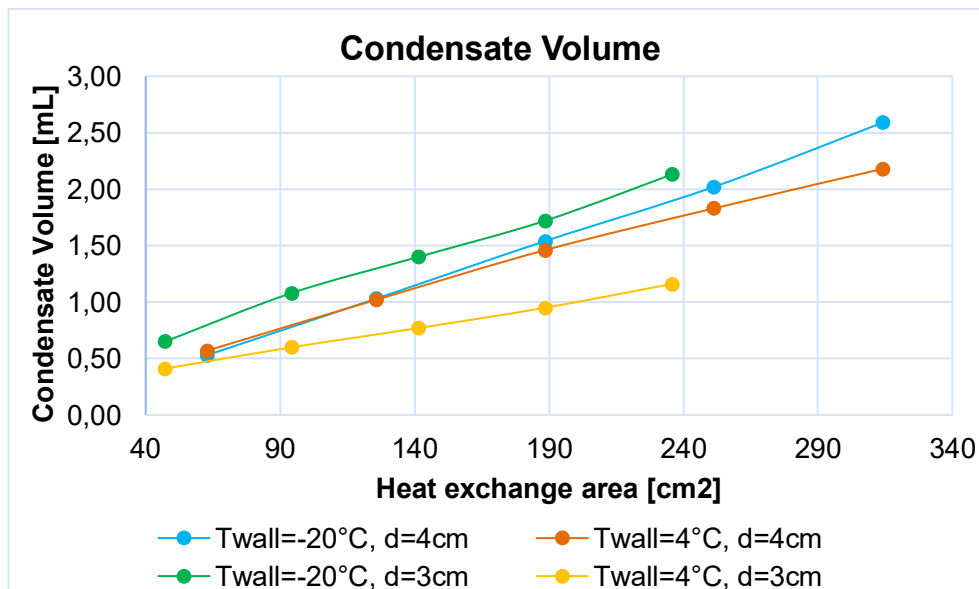


Figure 25. Condensate volume in the cylinder as the wall temperature and the cylinder diameter vary.

From this graph a condition of thermodynamic equilibrium was not reached in the cylinder during the simulation, because the volume of condensate continues to increase as the heat exchange area increases; a plateau has not been reached in which the volume no longer increases as the area of the cylinder wall changes. Therefore, it is not possible to have information on the exchange area and on the geometry of the condenser, because a minimum exchange area has not been identified that would allow maximizing the condensate yield.

Chapter 6: Conclusions and Future Developments

The use of Exhaled Breath Condensate (EBC) analysis in clinical practice is very promising and will have an evident positive impact due to the many advantages of this technique. First, it will have an impact on healthcare costs because this technique is cheaper than many other invasive tests and also the diagnose of lung diseases in the very early stage involves less treatment for the patient and therefore fewer costs. Furthermore, the condensate analysis will have a positive impact on the patient, who does not have to undergo invasive and risky examinations, some of which also require anaesthesia and for this reason he will be more favorable to undergo the examination and will carry it out more frequently during the follow-up. With this method it is possible to better follow the patient during the follow-up also because it can be carried out by patients of all ages, even with pathologies in an advanced stage.

In this thesis the condensation of a healthy subject exhaled air and the relative limits of the process have been studied in a situation of thermodynamic equilibrium of the system and in similar to reality condition. The condensation upon reaching equilibrium of the system was studied to choose the best thermodynamic model that could describe this process and has set a theoretical limit to the maximum yield obtainable in the condensate for the components of air and for the volume of condensate; with a CFD simulation, the exhaled breath condensation process was analysed from a fluid dynamics point of view after choosing a thermodynamic model, to evaluate the thermal exchange area with witch it is possible to reach a situation close to the equilibrium.

These analyses were carried out with the purpose to model an exhaled breath sampling and condensation system, aimed to the design of a first prototype; this can be used to evaluate specific biomarkers of lung diseases or to evaluate the presence of viral airway infections as viral DNA is collected in the condensate.

From this thesis work emerges that the condensate volume is in line with the values found in the literature. The concentration of ammonia in the EBC was highly dependent on the thermodynamic model used, although it could not be validated since the available data had an already large variability; this is due to the age and gender of the subjects from which they are collected, by their eating habits, by circadian rhythm, tobacco smoking and by the surrounding air [45] [20]. In the surrounding air there is dust, particulate or other

components, which affect the results of the measurements and make them subject to variations.

Moreover, from the analyses carried out in this thesis work and from the results obtained, a difficulty is denoted in defining a thermodynamic model suitable for the calculation of the properties of the phases, which leads to a difficulty in validating the results with the literature data. The thermodynamic equilibrium has been calculated between a gas and a liquid phase or between a gas and two liquid phases, without considering the formation of a solid phase, plausible due to low temperatures of the condenser because there are no classic models for study situations of this type.

As regards the CFD simulations, a validation for the condensate volume cannot be done because a condition of thermodynamic equilibrium was not reached in the cylinder and minimum exchange area has not been identified. This result is conditioned by the choice of an unsatisfactory thermodynamic model and by the impossibility of solid phase formation in the cylinder, set during the settings phase of the CFD simulation.

For the future developments of this study, it will be essential to better evaluate the thermodynamic model used to describe the condensation process to better fit the literature data obtained experimentally and choose a condensation model that allows to consider the solid phase formation inside the condenser. In particular, it will be useful to evaluate the models used for describing the freeze-drying process, a method to remove water from the condensate to obtain organic components with the minimum possible deterioration and to evaluate if the yield obtained with these methods better fits the data in the literature.

For the future work it will be necessary to better model the condensation process with CFD simulations, adding pieces of balance equations through the UDFs and to evaluate the geometry and the materials of the condenser with the aim of design and build a first prototype.

Appendix A: VOCs and Non-volatile Biomarkers for Lung Diseases

Compound	Physiological range	Evidence
Carbon Monoxide [10]	1 – 3 ppm	Increases in asthmatic patients, in subject with cystic fibrosis or bronchiectasis
Pentane [1] [10]	1 – 10 ppb	Increases in asthmatic patients or lung cancer patients
Nitric Oxide [10]	1 – 9 ppb	Increases in subject with asthma lung cancer or bronchiectasis, it does not change in subjects with COPD or chronic bronchitis, it decreases in people with cystic fibrosis
Isoprene [41]	80 – 100 ppb	It decreases in patients with cystic fibrosis, lung cancer or asthma
Hydrogen cyanide [1]	/	It increases in children with cystic fibrosis with <i>P. aeruginosa</i> infection
Sulphides [1]	/	It increases in children with cystic fibrosis with <i>P. aeruginosa</i> infection
Acetone [16] [42]	600 [177 – 2441] ppb	It increases in patients with lung cancer, decreases in covid-19 patients
Aldehydes: Pentanal Hexanal Octanal Nonanal [1]	0 - 0,011 0 - 0,001 0,004 -0,028 0,021 -0,096 nmol/L	Increase in patients with lung cancer
Ethane [1] [10]	0 – 10,54 ppb	It increases in patients with asthma, COPD or cystic fibrosis
Ethyl acetate [1]	1 – 8 ppb	It increases in patients with lung cancer
Benzene derivates [1]	/	It increases in patients with lung cancer
2-pentanone [1]	1 – 5,1 ppb	It increases in patients with lung cancer
2-propanol [1]	3 – 4 ppb	It increases in patients with lung cancer

Compound	Physiological range	Evidence
Ethylbutyrate [16]	/	It increases in subject with COVID-19
1-isopropanol [16]	/	Decreases in subject with COVID-19
Butyraldehyde and ethyl butanoate [16]	/	Both increase in subject with pathogen infections (no sars-cov-2), the first component decreases and the second increases in subjects affected by COVID-19
Methanol [43]	142 [50 – 500] ppb	It decreases in people with lung cancer
Ammonia [59]	0,5 – 2 ppm	Increases in asthmatic patients

Table A 1. VOCs biomarkers for lung diseases.

Compound	Physiological range in EBC	Evidence
Aldehydes: Malondialdehyd, Exanal, Heptanal, Nonanal [20] [21] [45]	12,1 – 35,6 17,7 – 64,9 14,2 – 29,6 14,8 – 18,7 nmol/L	Malondialdehyde increases in patents with asthma or COPD; Exanal, Heptanal, Nonanal increases in patents with COPD
pH [45]	7,4 – 8,8	It decreases in patients with asthma CF, COPD, bronchiectasis or ALI
Ammonia (NH ₃) [45]	14 – 1220 μmol/L	It increases in patients with asthma
IL-1 β , IL-2, IL-4, IL-5, IL-6, IL-8, IL-10, IL-17, IFN- γ , TGF- β , and TNF- α [27] [44]	~ 50 pg/mL	IL-6 increases in lung cancer, CF, COPD or asthma patients; IL-4, IL-8, IL-17, TNF- α increase in asthmatic patients; IFN- γ decrease in asthmatic patients; IL-8 is elevated in CF or COPD patients.
DNA – RNA [20]	/	Cellular DNA alterations are found in patients with lung cancer; presence of DNA and RNA in case of viral and bacterial lung infections.

Compound	Physiological range in EBC	Evidence
H ₂ O ₂ [45]	Max 0,9 µmol/L	Increases in patients with asthma, COPD, bronchiectasis, acute respiratory distress syndrome but not cystic fibrosis
Nitrates [45]	1 µmol/L	Increase in subjects with asthma, cystic fibrosis or bronchiectasis
Nitrites [45]	5 – 10 times higher than nitrites	Increase in subjects with asthma, cystic fibrosis, bronchiectasis or ALI
Nitrosothiol [45]	0,005 – 0,8 µmol/L	Increases in subjects with asthma or cystic fibrosis
Nitrotyrosine [45]	Max 14 ng/mL	Increases in subjects with asthma, cystic fibrosis or COPD
Adenosine [20] [45]	Max 20 nmol/L	Increases in subjects with asthma or cystic fibrosis
Prostaglandin E2 [20]	Max 75 pg/mL	Increases in subjects with COPD, ALI or ARDS
Leukotrienes [45]	Cys-LT: max 25 pg/mL LTB4: max 220 pg/mL	Increases in subjects with asthma or cystic fibrosis or COPD
8-isoprostane [20]	max 50 pg/mL	Increases in subjects with asthma, cystic fibrosis, COPD or ARDS

Table A 2. Non-volatile biomarkers for lung diseases.

Appendix B: Characteristics of Exhaled Breath Collecting and Condensing Devices on the Market and Self-made

	ECoScreen™ I	ECoScreen™ Turbo	RTube™	Turbo DECCS
Condensing temperature	-10°C/ -20°C	-4°C	-20°C/ -80°C	0/-10°C
Temperature control	Yes	Yes	No	Yes
Type of cooling system	electrical cooling system	electrical cooling system	Aluminium as cooling element	Peltier-type electrical cooling system
Type of condensing camera	Close	Close	Open	Close
Condensing camera material	PTFE	PE	PP	/
Conducting tube material	/	/	Not present	PP o PE
Portability	Semi-portable	Semi-portable	Portable	Semi-portable
Cost	Higher then RTube™	Higher then RTube™	Low	/
Recommended/ used collection time	5 – 10 minutes	5 – 10 minutes	10 minutes	10 – 15 minutes
Exhaled air volume (L)	105	/	106	Min 50
Collected EBC volume (mL)	1	/	1	1,5 – 3,0
Additional components	Saliva filter and two-way valve to separate inhaled and exhaled air integrated, Ecovent	Saliva filter and integrated two-way valve to separate inhaled and exhaled air, Ecovent	Integratd one-way valve, saliva trap	Integrated saliva trap

Table B 1. Characteristics of exhaled breath collecting and condensing devices on the market [44] [50] [51] [52] [53] [57] [58].



Figure B 1. Sampling device ECoScreen™ [20].

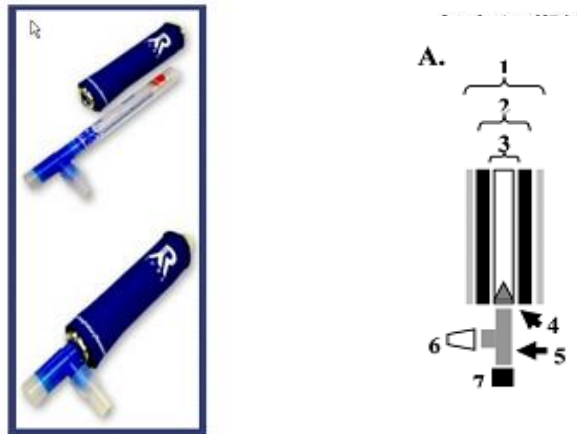


Figure B 2. A) Sampling device RTube™ B) RTube™ components scheme: 1. Insulator, 2. Aluminium sleeve, 3. Condensing tube, 4. One-way valve, 5. T-connector, 6. Mouthpiece and 7. Saliva trap [44] [52].



Figure B 3. Sampling device Turbo DECCS [XV].

	Modified RTube™ EBC collection apparatus (Figure B4)	RTube™ and Loccioni instrument (Figure B5)	Teflon PFA tube in ice bucket condensing system (Figure B6)	Glass condensing system (Figure B7)
Condensing temperature	4°C	-78°C	/	/
Temperature control	As for RTube™	As for RTube™	No	No
Type of cooling system	As for RTube™	Dry ice around the aluminium coating as cooling system	Ice as cooling element	Ice as cooling element
Type of condensing camera	As for RTube™	As for RTube™	Open	Close
Condensing camera material	As for RTube™	As for RTube™	PP	Glass
Conducting tube material	/	/	Teflon PFA	/
Portability	Not portable	Semi-portable	Semi-portable	Semi-portable
Cost	Higher than RTube™	Low	Low	Low
Recommended/used collection time	5 minutes	6 or 10 minutes	5 minutes	15 minutes
Exhaled air volume (L)	Mean 53	/	/	/
Collected EBC volume (mL)	Mean 0,54	About 0.8 for 6 minutes and about 1,5 for 10 minutes	1	1
Components	EcoVent, HEPA filter, incentive spirometer	Respir-guard 303 filter, CO2 sensor, coating for the condensation chamber	/	Saliva trap, one-way valve at the outlet

Table B 2. Characteristics of exhaled breath collecting and condensing self-made devices [52] [54] [55] [56].

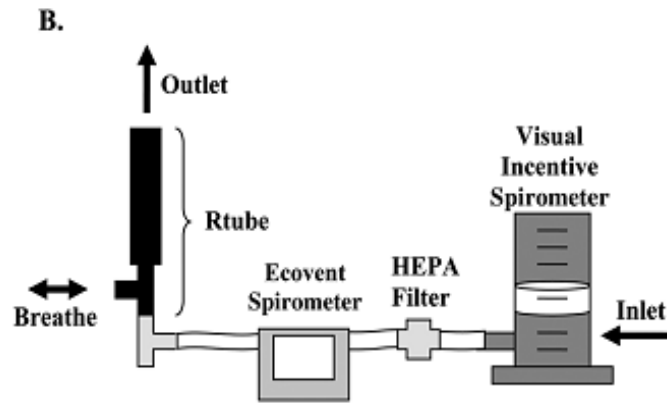


Figure B 4. Modified RTube EBC collection apparatus [52].

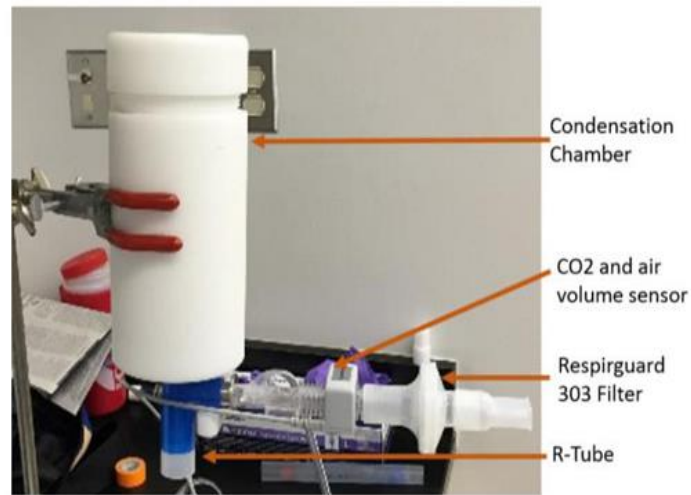


Figure B 5. RTube™ and Loccioni instrument [54].

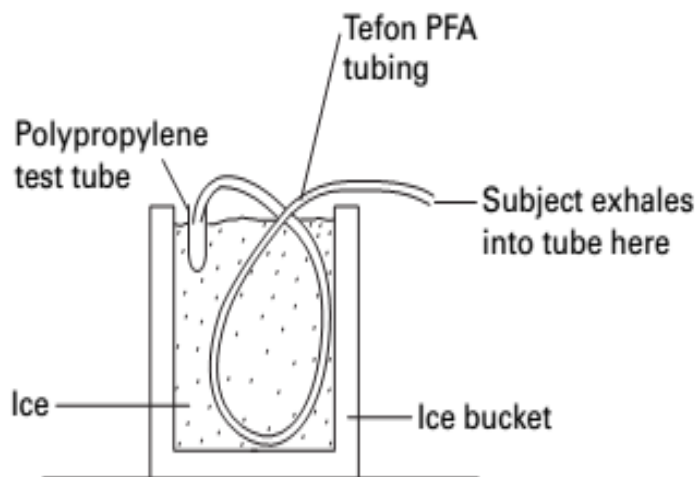


Figure B 6. Teflon PFA tube in ice bucket condensing system [55].

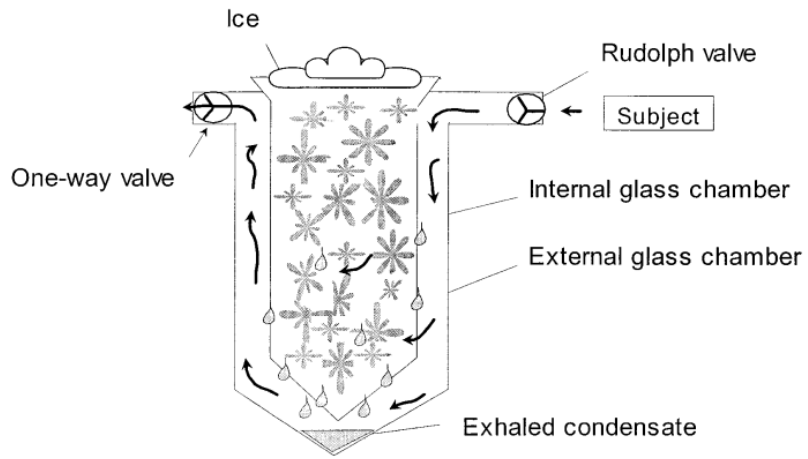


Figure B 7. Glass condensing system [56].

Bibliography

- [1] K. D. van de Kant, L. J. van der Sande, Q. Jöbssis e al., «Clinical use of exhaled volatile organic compounds in pulmonary diseases: a systematic review,» *Respiratory Research*, vol. 13, n. 1, p. 117, 2012.
- [2] A. Villaseñor, D. Rosace, D. Obeso e al., «Allergic asthma: an overview of metabolomic strategies leading to the identification of biomarkers in the field,» *Clinical et Experimental Allergy*, vol. 47, pp. 442-456, 2017.
- [3] P. Campi, L. Emmi, A. Matucci e al., «Linee guida sull'asma bronchiale,» *SNLG-Regioni*, vol. 1, pp. 9-24, 2014.
- [4] J. Vestbo, S. S. Hurd, A. G. Agusti e al., «Global Strategy for the Diagnosis, Management and Prevention of Chronic Obstructive Pulmonary Disease,» *American Journal of Respiratory and Critical Care Medicine*, vol. 187, n. 4, 2012.
- [5] M. M. Rafeeq e H. A. S. Murad, «Cystic fibrosis: current therapeutic targets and future approaches. Journal of Translational Medicine,» vol. 15, n. 1, p. 84, 2017.
- [6] E. T. Kanik, O. Yilmaz, E. Ozdogru e al., «Relevance between clinical status and exhaled molecules related to neutrophilic inflammation in pediatric cystic fibrosis,» *Journal of Breath Research*, vol. 14, n. 4: 046007, 2020.
- [7] G. M. Pontieri, «Principali patologie dell'apparato respiratorio,» in *Patologia generale & fisiopatologia generale*, Padova, Piccin Nuova Libreria, 2017.
- [8] Y. Yang, M. Yang, C. Shen e al., «Evaluating the accuracy of different respiratory specimens in the laboratory diagnosis and monitoring the viral shedding of 2019-nCoV infections,» *medRxiv*, 2020.
- [9] C. Huang, Y. Wang, X. Li e al., «Clinical features of patients infected with 2019 novel coronavirus in Wuhan, China,» *The Lancet*, vol. 395, n. 10223, pp. 497-506, 2020.
- [10] S. A. Kharitonov e P. J. Barnes, «Exhaled markers of pulmonary disease,» *American Journal of Respiratory and Critical Care*

Medicine, vol. 163, n. 7, pp. 1693-1722., 2001.

- [11] J. Diaz-Mendoza, A. R. Peralta, L. Debiane e al., «Rigid Bronchoscopy,» *Seminars in Respiratory and Critical Care Medicine*, vol. 39, pp. 674-684, 2018.
- [12] R. J. Miller, R. F. Casal, D. R. Lazarus e al., «Flexible Bronchoscopy,» *Clinics in Chest Medicine*, vol. 39, n. 1, pp. 1-16, 2018.
- [13] J. G. Shaw, A. Vaughan, A. G. Dent e al., «Biomarkers of progression of chronic obstructive pulmonary disease (COPD),» *Journal of Thoracic Disease*, vol. 6, n. 11, pp. 1532-1547, 2014.
- [14] W. Wang, Y. Xu, R. Gao e al., «Detection of SARS-CoV-2 in Different Types of Clinical Specimens,» *Journal of American Medical Association*, vol. 323, n. 18, pp. 1843-1844, 2020.
- [15] K. K. W. To, O. T. Y. Tsang, C. C. Y. Yip e al., «Consistent Detection of 2019,» *Clinical Infectious Diseases*, vol. 71, n. 15, p. 841 –843, 2020.
- [16] H. Chen, X. Qi, J. Ma e al., «Breath-borne VOC Biomarkers for COVID-19,» *medRxiv*, 2020.
- [17] T. Zitek, «The Appropriate Use of Testing for COVID-19,» *The western journal of Emergency Medicine*, vol. 21, n. 3, pp. 470-472, 2020.
- [18] G. Rao e E. Vejerano, «Partitioning of volatile organic compounds to aerosols: A review,» *Chemosphere*, vol. 212, pp. 282-296, 2018.
- [19] Z. L. Borrill, K. Roy e D. Singh, «Exhaled breath condensate biomarkers in,» *The European respiratory journal*, vol. 32, n. 2, p. 472–486, 2008.
- [20] H. Ahmadzai, S. Huang, R. Hettiarachchi e al., «Exhaled breath condensate: a comprehensive update,» *Clinical chemistry and laboratory medicine*, vol. 51, n. 7, pp. 1343-1361, 2013.
- [21] M. Corradi, I. Rubinstein, R. Andreoli e al., «Aldehydes in Exhaled Breath Condensate of Patients with Chronic Obstructive Pulmonary Disease,» *American Journal of Respiratory and Critical Care Medicine*, vol. 167, pp. 1380-1386, 2003.

- [22] F. C. Mendes, I. Paciência, A. C. Ferreira e al., «Development and validation of exhaled breath condensate microRNAs to identify and endotype asthma in children,» *Plos one*, vol. 14, n. 11: e0224983, 2019.
- [23] B. Pattnaik, P. B. Sryma, S. Mittal e al., «MicroRNAs in pulmonary sarcoidosis: A systematic review,» *Respiratory Investigation*, vol. 58, pp. 232-238, 2020.
- [24] M. Khoubnasabjafari, V. Jouyban-Gharamaleki, R. Ghanbari e al., «Exhaled breath condensate as a potential specimen for diagnosing COVID-19,» *Bioanalysis*, 2020.
- [25] S. Patsiris, T. Exarchos e P. Vlamos, «Exhaled Breath Condensate (EBC): Is It a Viable Source of Biomarkers for Lung Diseases?,» *Advances in Experimental Medicine and Biology*, vol. 1195, pp. 13-18, 2020.
- [26] G. M. Mutlu, K. W. Garey, R. A. Robbins e al., «Collection and Analysis of Exhaled Breath Condensate in Humans,» *American journal of respiratory and critical care medicine*, vol. 164, pp. 731-737, 2001.
- [27] Y. Liang, S. M. Yeligar e L. A. S. Brown, «Exhaled Breath Condensate: A Promising Source for Biomarkers of Lung Disease,» *The Scientific World Journal*, vol. 2012, pp. 1-7, 2012.
- [28] W. Gordon, «Thermodynamics,» *Encyclopedia Britannica*, 23 Jul. 2020.
- [29] P. Atkins e J. de Paula, *Chimica Fisica*, Bologna: Zanichelli editore S.p.A., 2012.
- [30] AspenTech, «Aspen Physical Property System-V8.4,» Burlington, MA, 2013.
- [31] P. Zanello, S. Mangani e G. Valensin, *Le basi della chimica*, Milano: Case Editrice Ambrosiana, 2001.
- [32] Y. Hussain, «Thermodynamic Models & Physical Properties».
- [33] E. C. Carlson, «Don't Gamble With Physical Properties For Simulations,» *Chemical Engineering progress*, pp. 35-46, 1996.
- [34] A. Giordano, A. Barresi e D. Fissore, «On the Use of Mathematical Models to Build the Design Space for the Primary

Drying Phase of a Pharmaceutical Lyophilization Process,»
Journal of Pharmaceutical Sciences, vol. 100, n. 1, pp. 311-324,
2011.

- [35] D. Fissore, R. Pisano e A. Barresi, «On the Methods Based on the Pressure Rise Test for Monitoring a Freeze-Drying Process,»
Drying Technology: An International Journal, vol. 29, n. 1, pp. 73-90, 2010.
- [36] O. Gould, N. Ratcliffe, E. Król e al., «Breath analysis for detection of viral infection, the current position of the field,»
Journal of Breath Research, vol. 14, n. 4: 041001, 2020.
- [37] G. Carpagnano, D. Lacedonia, M. Natalicchio e al., «Viral colonization in exhaled breath condensate of lung cancer,» *The Clinical Respiratory Journal*, vol. 0, pp. 00-00, 2016.
- [38] L. Houspie, S. De Coster, E. Keyaerts e al., «Exhaled breath condensate sampling is not a new method for detection of respiratory viruses,» *Virology Journal*, vol. 8, p. 98, 2011.
- [39] G. Carpagnano, A. Koutelou, M. Nataliccio e al., «HPV in exhaled breath condensate of lung cancer patients,» *British Journal of Cancer*, vol. 105, pp. 1183-1190, 2011.
- [40] J. Hunt, «Exhaled Breath Condensate: An Overview,»
Immunology and Allergy Clinics of North America, vol. 27, pp. 587-596, 2007.
- [41] J. King, A. Kupferthaler, K. Unterkofler e al., «Isoprene and acetone concentration profiles during exercise on an ergometer,» *Journal of Breath Research*, vol. 3, n. 2: 027006, 2009.
- [42] K. Schwarz, A. Pizzini, B. Arendacka e al., «Breath acetone-aspects of normal physiology related to age and gender as determined in a PTR-MS study,» *Journal of*, vol. 3, n. 027003, 2009.
- [43] A. Bajtarevic, C. Clemens Ager, M. Pienz e al., «Noninvasive detection of lung cancer by analysis of exhaled breath,» *BMC Cancer*, vol. 9, n. 348, 2009.
- [44] P. Kubáň e F. Foret, «Exhaled breath condensate: Determination of non-volatile compounds and their potential for clinical diagnosis and monitoring. A review.,» *Analytica Chimica*

Acta, vol. 805, pp. 1-18, 2013.

- [45] I. Horváth, J. Hunt e P. J. Barnes, «Exhaled breath condensate: methodological recommendations and unresolved questions,» *European Respiratory Journal*, vol. 26, pp. 523-548, 2005.
- [46] D. U. Silverthorn, «Mechanics of Breathing,» in *Human Physiology: An Integrated Approach*, Pearson, 7th Edition, 2015.
- [47] J. D. Johnson e W. M. Theurer, «A Stepwise Approach to the Interpretation of Pulmonary Function Tests,» *American Family Physician*, vol. 89, n. 5, pp. 359-366, 2014.
- [48] J. Vestbo, S. S. Hurd, A. G. Agusti e al., «Global Strategy for the Diagnosis, Management and Prevention of Chronic Obstructive Pulmonary Disease: GOLD executive summary,» *American Journal of Respiratory and Critical Care Medicine*, vol. 187, n. 4, pp. 347-365, 2012.
- [49] A. Rybacka, J. Goździk-Spychalska, A. Rybacki e al., «Congruence Between Pulmonary Function and Computed Tomography Imaging Assessment of Cystic Fibrosis Severity,» *Advances in Experimental Medicine and Biology*, vol. 1114, pp. 67-76, 2018.
- [50] O. Soyer, E. A. Dizdar, O. Keskin e al., «Comparison of two methods for exhaled breath condensate collection,» *Allergy*, vol. 61, n. 8, pp. 1016-1018, 2006.
- [51] E. M. Hüttmann, T. Greulich, A. Hattesoehl e al., «Comparison of Two Devices and Two Breathing Patterns for Exhaled Breath Condensate Sampling,» *Plos One*, vol. 6, n. 11: e27467, 2011.
- [52] J. R. Fox, E. W. Spannhake, K. K. Macri e al., «Characterization of a portable method for the collection of exhaled breath condensate and subsequent analysis of metal content,» *Environmental Science: Processes & Impacts*, vol. 15, n. 4, pp. 721-729, 2013.
- [53] S. R. Carter, C. S. Davis e E. J. Kovacs, «Exhaled breath condensate collection in the mechanically ventilated patient,» *Respiratory Medicine*, vol. 106, n. 5, pp. 601-613, 2012.
- [54] B. R. Winters, J. D. Pleil, M. M. Angrish e al., «Standardization of the collection of exhaled breath condensate and exhaled breath

aerosol using a feedback regulated sampling device,» *Journal of Breath Research*, vol. 11, n. 4: 047107, 2018.

- [55] L. P. Ho, J. A. Innes e A. P. Greening, «Nitrite levels in breath condensate of patients with cystic fibrosis is elevated in contrast to exhaled nitric oxide,» *Thorax*, vol. 53, n. 8, pp. 680-684, 1998.
- [56] I. Horváth, L. E. Donnelly, A. Kiss e al., «Combined Use of Exhaled Hydrogen Peroxide and Nitric Oxide in Monitoring Asthma,» *American Journal of Respiratory and Critical Care Medicine*, vol. 158, n. 4, pp. 1042-1046, 1998.
- [57] C. Gessner, H. Kuhn, H.-J. Seyfarth e al., «Factors influencing breath condensate volume,» *Pneumologie*, vol. 55, n. 9, pp. 414-419, 2001.
- [58] K. O. Zamuruyev, A. A. Aksenov, A. Pasamontes e al., «Human breath metabolomics using an optimized non-invasive exhaled breath condensate sampler,» *Journal of Breath Research*, vol. 11, n. 1: 016001, 2017.
- [59] T. L. Mathew, P. Pownraj, S. Abdulla e al., «Technologies for clinical diagnosis using expired human breath analysis,» *Diagnostics*, vol. 5, pp. 27-60, 2015.
- [60] R. A. Theye, «Chromatographic analysis of expired air containing halothane,» *Anesthesiology*, vol. 25, n. 1, pp. 75-79, 1964.
- [61] S. Tarantola, A. Saltelli, F. Campolongo e M. Ratto, *Sensitivity Analysis in Practice: A Guide to Assessing Scientific Models*, John Wiley & Sons, Ltd, 2004.
- [62] R. C. Giwa e A. Anene, «Modelling, Simulation and Sensitivity Analysis of a Fatty Acid Methyl Ester Reactive Distillation Process Using Aspen Plus,» *International Journal of Engineering Research in Africa*, vol. 27, pp. 36-50, 2016.
- [63] J. F. Hunt, E. Erwin, L. Palmer e al., «Expression and Activity of pH-regulatory Glutaminase in the Human Airway Epithelium,» *American Journal of Respiratory and Critical Care Medicine*, vol. 165, pp. 101-107, 2002.
- [64] M. Lecuna, *Scale down of a dynamic generator of VOC reference gas mixtures*, Torino: Politecnico di Torino, 2017.

- [65] F. M. Schmidt, O. Vaittinen e M. Metsala, «Ammonia in breath and emitted from skin,» *Journal of breath research*, vol. 7, n. 017109, 2013.
- [66] Q. Yi, M. Tian e D. Fang, «CFD Simulation of air-steam condensation on an isothermal,» *INTERNATIONAL JOURNAL OF HEAT AND TECHNOLOGY*, vol. 33, n. 1, pp. 25-32, 2015.
- [67] D. Yoon, H. Jo e M. Corradini, «CFD modeling of filmwise steam condensation with noncondensable gas with modified boundary condition,» *International Journal of Heat and Mass Transfer*, vol. 125, pp. 485-493, 2018.
- [68] D. Sun, J. Xu e Q. Chen, «Modeling of the Evaporation and Condensation Phase-Change Problems with FLUENT,» *Numerical Heat Transfer, Part B: Fundamentals*, vol. 66, n. 4, pp. 326-342, 2014.
- [69] N. Tiller e A. Simpson, «Effect of spirometry on intra-thoracic,» *BMC Research Notes*, vol. 11, n. 110, 2018.
- [70] W. Oberkampf e T. Trucano, «Verification and validation in computational fluid dynamics,» *Progress in Aerospace Sciences*, vol. 38, pp. 209-272, 2002.

Sitography

- [I] <https://www.who.int/news-room/fact-sheets/detail/the-top-10-causes-of-death>
- [II] <https://www.who.int/news-room/fact-sheets/detail/cancer>
- [III] <https://gco.iarc.fr/today/home>
- [IV] <https://www.cff.org/What-is-CF/About-Cystic-Fibrosis/>
- [V] <https://www.uchicagomedicine.org/conditions-services/lung-diseases/interstitial-lung-disease-pulmonary-fibrosis>
- [VI] <https://www.nhlbi.nih.gov/health-topics/acute-respiratory-distress-syndrome>
- [VII] <https://clinical.r-biopharm.com/it/indicazioni/infezioni-respiratorie/>
- [VIII] <https://www.fondazioneveronesi.it/magazine/tools-della-salute/glossario-delle-malattie/influenza>
- [IX] <http://www.salute.gov.it/portale/nuovocoronavirus/dettaglioNotizieNuovoCoronavirus.jsp?menu=notizie&id=4067>
- [X] <https://www.who.int/dg/speeches/detail/who-director-general-s-opening-remarks-at-the-media-briefing-on-covid-19---11-march-2020>
- [XI] <https://covid19.who.int/>
- [XII] <https://www.cdc.gov/coronavirus/2019-ncov/lab/guidelines-clinical-specimens.html>
- [XIII] [Water Vapor Pressure Formulations \(colorado.edu\)](#)
- [XIV] <https://www.healthline.com/health/spirometry>
- [XV] <http://www.medivac.it/turbo-deccs-systems/>
- [XVI] <http://www.flycarpet.net/en/psyonline>
- [XVII] <https://www.itl.nist.gov/div898/handbook/eda/section3/eda3662.htm>
- [XVIII] [metrologia 07-temperatura.ppt \(infn.it\)](#)
- [XIX] <http://www.meteovalleditria.it/files/MeteorologiaSinottica3.pdf>
- [XX] [RTube™ Exhaled Breath Condensate Collection Device \(respiratoryresearch.com\)](#)